

# Bright globular clusters in NGC 5128: the missing link between young massive clusters and evolved massive objects<sup>★</sup>

M. Rejkuba<sup>1</sup>, P. Dubath<sup>2,3</sup>, D. Minniti<sup>4</sup>, and G. Meylan<sup>5</sup>

<sup>1</sup> ESO, Karl-Schwarzschild-Strasse 2, D-85748 Garching, Germany  
e-mail: mrejkuba@eso.org

<sup>2</sup> Observatoire de Genève, ch. des Maillettes 51, CH-1290 Sauverny, Switzerland

<sup>3</sup> INTEGRAL Science Data Centre, ch. d'Ecogia 16, CH-1290 Versoix, Switzerland  
e-mail: pierre.dubath@obs.unige.ch

<sup>4</sup> Department of Astronomy and Astrophysics, Pontificia Universidad Católica de Chile, Vicuña Mackenna 4860, Santiago 22, Chile  
e-mail: dante@astro.puc.cl

<sup>5</sup> Ecole Polytechnique Fédérale de Lausanne (EPFL), Observatoire, CH-1290 Sauverny, Switzerland  
e-mail: georges.meylan@epfl.ch

Received 01 October 2006; accepted 13 March 2007

## ABSTRACT

**Context.** Globular clusters are the simplest stellar systems in which structural parameters are found to correlate with their masses and luminosities.

**Aims.** In order to investigate whether the brightest globular clusters in the giant elliptical galaxies are similar to the less luminous globular clusters like those found in Local Group galaxies, we study the velocity dispersion and structural parameter correlations of a sample of bright globular clusters in the nearest giant elliptical galaxy NGC 5128 (Centaurus A).

**Methods.** UVES echelle spectrograph on the ESO Very Large Telescope (VLT) was used to obtain high resolution spectra of 23 bright globular clusters in NGC 5128, and 10 clusters were observed with EMMI in echelle mode with the ESO New Technology Telescope. The two datasets have 5 clusters in common, while one cluster observed with UVES had too low signal-to-noise (S/N). Hence the total number of clusters analysed in this work is 27, more than doubling the previously known sample. Their spectra were cross-correlated with template spectra to measure the central velocity dispersion for each target. The structural parameters were either taken from the existing literature, or in cases where this was not available, we have derived them from our VLT FORS1 images taken under excellent seeing conditions, using the ISHAPE software. The velocity dispersion and structural parameter measurements were used to obtain masses and mass-to-luminosity ratios ( $M/L_V$ ) of 22 clusters.

**Results.** The masses of the clusters in our sample range from  $M_{vir} = 10^5 - 10^7 M_\odot$  and the average  $M/L_V$  is  $3 \pm 1$ . The three globular clusters harbouring X-ray point sources are the second, third and sixth most massive in our sample. The most massive cluster, HCH99-18, is also the brightest and the largest in size. It has the mass ( $M_{vir} = 1.4 \times 10^7 M_\odot$ ) an order of magnitude larger than the most massive clusters in the Local Group, and a high  $M/L_V$  ratio ( $4.7 \pm 1.2$ ). We discuss briefly possible formation scenarios for this object.

**Conclusions.** The correlations of structural parameters, velocity dispersion, masses and  $M/L_V$  for the bright globular clusters in NGC 5128 extend the properties established for the most massive Local Group clusters towards those characteristic of dwarf elliptical galaxy nuclei and Ultra Compact Dwarfs (UCDs). The detection of the mass–radius and the mass– $M/L_V$  relations for the globular clusters with masses greater than  $\sim 2 \times 10^6 M_\odot$  provides the missing link between “normal” old globular clusters, young massive clusters, and evolved objects like UCDs.

**Key words.** Galaxies: elliptical and lenticular, cD – Galaxies: Individual: NGC 5128 – Galaxies: star clusters

## 1. Introduction

The properties of globular clusters and the observed correlations between their various internal structural and dynamical parameters offer empirical constraints not only on the formation of globular clusters themselves, but also on the his-

tory of the host galaxy. A large number of empirical relations between various properties, core and half-light radii, surface brightnesses, velocity dispersions, concentrations, luminosities, metallicities, etc., of the Milky Way globular clusters have been found (e.g. Djorgovski & Meylan 1994). Many of them are mutually dependent due to the fact that globular clusters have remarkably simple structures that can be reasonably well approximated by isotropic, single-mass King (1966) models. McLaughlin (2000) has shown that the Milky Way clusters are confined to the fundamental plane well defined by 2 empiri-

Send offprint requests to: M. Rejkuba

<sup>★</sup> Based on observations collected at the European Southern Observatory, Paranal, Chile, within the Observing Programmes 63.N-0229 and 069.D-0169.

cal relations:  $M/L = \text{const.}$  and  $E_b \sim L^{2.05}$ , where  $M$  is the mass,  $L$  the luminosity, and  $E_b$  the binding energy of the cluster.

The brightest and the most massive globular cluster of our Galaxy,  $\omega$  Cen (Meylan et al. 1995), is peculiar in many of its characteristics: e.g. it is the most flattened Galactic globular cluster (White & Shawl 1987) and it shows strong variations in nearly all element abundances (e.g. Norris & Da Costa 1995; Pancino et al. 2002). A scenario that may explain some of its characteristics is that  $\omega$  Cen is the nucleus of a former dwarf elliptical galaxy (Zinnecker et al. 1988; Hughes & Wallerstein 2000; Hilker & Richtler 2000). The same scenario was proposed for M54, another very massive globular cluster. It is a candidate for the nucleus of the Sagittarius dwarf (e.g. Bassino & Muzzio 1995; Layden & Sarajedini 2000), a galaxy that is currently being accreted by the Milky Way. M31 has 4 globular clusters for which Djorgovski et al. (1997) measured velocity dispersions  $\sigma > 20 \text{ km s}^{-1}$  implying masses at least as large as the one of  $\omega$  Cen. The most massive of them, G1, shares also other particular properties of  $\omega$  Cen, like the flattening and metallicity dispersion (Meylan et al. 2001). From the recent work of Ma et al. (2006), the most luminous M31 globular cluster, 037-B327, has been suggested to be the most massive Local Group cluster, with a total mass of  $(3.0 \pm 0.5) \times 10^7 \text{ M}_\odot$ , determined photometrically. These authors estimate the (one-dimensional) velocity dispersion for 037-B327 of  $(72 \pm 13 \text{ km s}^{-1})$ . However, a later paper by Cohen (2006) challenged this result, based on the measured velocity dispersion of  $\sigma = 21.3 \pm 0.4 \text{ km s}^{-1}$ , which is comparable to that of G1 ( $\sigma = 25.1 \pm 0.3 \text{ km s}^{-1}$ ; Djorgovski et al. 1997). She concluded that 037-B327 is not the most massive cluster in the Local Group, and that probably M31 clusters G1, G78 and G280 are more massive than 037-B327. Going to galaxies beyond the Local Group, very similar to G1 in M31 is the cluster n1023-13 in NGC 1023 (Larsen 2001).

With luminosities and masses larger than globular clusters are the so-called ultra compact dwarfs (UCDs) or dwarf-globular transition objects (DGTOs) discovered in Fornax and Virgo galaxy clusters (Hilker et al. 1999; Drinkwater et al. 2000; Haşegan et al. 2005; Hilker et al. 2007). While their origin and relation to globular clusters is still debated in the literature, it has been established that very massive young star clusters can form in major star forming events. Such clusters, with masses of the order of  $> 10^6$ , or even  $> 10^7 \text{ M}_\odot$  (Maraston et al. 2004; Bastian et al. 2006), show similar scaling relations as UCDs/DGTOs, but might be different from the less massive globular clusters based on examination of their mass-velocity dispersion and mass-radius relations (Kissler-Patig et al. 2006). However, we point out that the ages of UCDs/DGTOs are similar to those of globular clusters, in contrast to the massive young star clusters forming in mergers.

To populate the transition region between “normal” globular clusters and more massive DGTOs, it is of interest to look at the massive elliptical galaxies which harbour globular cluster systems which are an order of magnitude more populous than those of the Local Group spiral galaxies. The nearest easily observable elliptical galaxy is NGC 5128. It has a large number of bright globular clusters with luminosities exceeding the brightest Local Group globulars. This makes it an ideal target.

The most recent distance determination to this galaxy is  $3.42 \pm 0.18 \pm 0.25 \text{ Mpc}$  (the first is random and the second systematic error), obtained using Cepheid PL relation (Ferrarese et al. 2006). Here we use the distance of  $3.84 \pm 0.35 \text{ Mpc}$  (Rejkuba 2004), which is the same value used in a previous work by Martini & Ho (2004) who presented velocity dispersions and mass-to-light ratios for 14 bright globular clusters in NGC 5128. In this work we present new high resolution spectra and derive M/L ratios, thus more than doubling the sample of bright globular clusters with similar data in the literature.

A decade ago Dubath (1994) presented at a conference the first measurements of velocity dispersions of 10 bright globular clusters in NGC 5128. Since these results have not been published in a refereed journal yet, they are included here along with the more recent observations of 23 clusters from UVES high-resolution echelle spectrograph of ESO Kueyen (UT2) telescope of Very Large Telescope (VLT).

This paper is organized as follows: Sect. 2 describes the observations and data reduction, Sect. 3.1 shows the results of the cross-correlation technique for radial velocity and metallicity standard stars, while Sect. 3.2 presents the results from the radial velocity and core velocity dispersion measurements of globular clusters in NGC 5128. The comparison with previous measurements of clusters’ radial velocity and velocity dispersion is in Sect. 3.2.1. In Sect. 4 the structural parameters for 22 clusters are presented. For those clusters which had no previous determinations of structural parameters in the literature we derive them from our high resolution ground-based images fitting the King profile (King 1962) using ISHAPE (Larsen 1999, 2001) programme. In Sect. 5 we derive mass-to-luminosity ratios for the clusters and in Sect. 7 discuss the correlations and fundamental plane. Finally, in Sect. 8 we summarize our results.

## 2. Sample selection and observations

The observations of 10 bright clusters (selected from the lists of van den Bergh et al. 1981; Hesser et al. 1986; Harris et al. 1992) were taken in March-April 1993 with the echelle mode of EMMI (Dekker et al. 1986), the multi-mode instrument of the ESO New Technology Telescope (NTT). These data have previously been presented at a conference (Dubath 1994), and are published here together with the observations of 23 clusters obtained with UVES echelle spectrograph (Dekker et al. 2000) of the ESO VLT in April 2002. There are 5 clusters observed with both instruments and these have been used to check for the systematics in the data and errors.

The sample of globular clusters selected for observations with UVES contains the brightest NGC 5128 clusters with either membership confirmed through published radial velocities (van den Bergh et al. 1981; Hesser et al. 1986; Harris et al. 1992, cluster names starting with VHH81, HHH86, and HGHH92) or the structural parameters and colours typical for globular clusters in the Milky Way (Holland et al. 1999; Rejkuba 2001, cluster names starting with HCH99 and with R, respectively).

## 2.1. EMMI spectroscopy

The first high-resolution integrated-light spectra of bright globular clusters in NGC 5128 were obtained with EMMI at ESO NTT telescope during three nights, March 31 to April 2 1993. The red arm of EMMI was used in Echelle mode (REMD) with grating #10 and grism #3 (CD2), yielding the resolving power of 30,000, corresponding to  $10 \text{ km s}^{-1}$ , and the wavelength coverage was from 4500 to 9000 Å, divided among 65 useful orders.

In total 14 spectra of 10 of the brightest globular clusters, selected from the catalogues of van den Bergh et al. (1981), Hesser et al. (1984), and Harris et al. (1992), were secured. The ThAr calibration lamp spectra were taken before and after each cluster spectrum. In addition, the following four K giant radial velocity standard stars were observed on each of the three nights: NGC 2447-s28, NGC 2447-s4, HD 171391 and HD 176047. All the spectra were reduced with the INTERTACOS software developed by Queloz & Weber in Geneva Observatory (see e.g. Queloz et al. 1995).

## 2.2. UVES spectroscopy

The UVES observations were carried out on the nights of 19 and 20 April 2002 in visitor mode. The red arm of UVES spectrograph was used with the standard CD#3 setting centered on 580 nm. It is equipped with two CCDs, covering the total wavelength range from 4760 Å to 6840 Å, with a gap of 50 Å centered on 5800 Å. The slit was 1" wide, giving the resolution of  $\lambda/\Delta\lambda \sim 42,000$ . The sky conditions were clear and the seeing varied between 0'.6 to 1'.3, but it stayed most of the time around 0'.8.

Globular clusters observed with UVES have *V*-band magnitudes ranging from 17.1 to 18.8 for 22 clusters. The faintest observed cluster had *V* = 19.44. The typical exposure times were 1200 sec for the brighter or 1800 sec for the fainter clusters, except for the faintest 19.4 mag cluster which was exposed for 2700 sec. Four clusters have been observed twice and one cluster three times during the two night run. The multiple exposures have been averaged to increase the signal-to-noise (S/N), but were also reduced independently in order to provide estimates of measurement errors. The observation log for all the clusters is in Table 1, where we list (1) the name, (2) the observation date, (3) the exposure times in seconds, (4) the typical S/N measured on the blue side of the  $H_\alpha$  line at  $\sim 6550$  Å using the *splot* IRAF task. The last column lists the *V* magnitude of the clusters taken from the literature.

Apart from the globular cluster targets, we have observed 17 different G and K-type giant stars with a range of metallicities ( $-2.6 < [\text{Fe}/\text{H}] < +0.3$  dex) to be used as templates for cross-correlation. Some stars were observed several times, thus yielding a total of 28 high S/N stellar spectra. The observation log of the template stars is in Table 2.

After each target spectrum, globular cluster or star, we have obtained the ThAr lamp spectrum at the same telescope position. The bias and flat-field calibration data were taken at the end of each night.

**Table 1.** Observations log for globular clusters: observations in 1993 were done with EMMI at NTT and in 2002 with UVES at Kueyen VLT. The nomenclature of the clusters is following that of the Peng et al. (2004a) catalogue, and the magnitudes given in the last column are from the same catalogue where available. For the clusters for which there are no measurements in that catalogue, we take the magnitudes from the original discovery publications.

(1) ID	(2) Date yyyy-mm-dd	(3) Exp. sec	(4) S/N@ 6550Å	(5) V mag
HGHH92-C1	1993-04-02	4800		17.42
HGHH92-C1	2002-04-20	1200	4	17.42
HGHH92-C1	2002-04-20	1200	4.5	17.42
VHH81-C3	1993-04-01	4800		17.71
VHH81-C5	1993-04-02	4800		17.68
HGHH92-C6	1993-03-31	3600		17.21
HGHH92-C6	1993-04-01	4200		17.21
HGHH92-C7	1993-03-31	3060		17.17
HGHH92-C7	1993-03-31	3600		17.17
HGHH92-C7	2002-04-19	1200	10	17.17
HGHH92-C7	2002-04-19	1200	11	17.17
HGHH92-C7	2002-04-20	1200	11	17.17
HGHH92-C11	2002-04-20	1200	6	17.91
HGHH92-C11	2002-04-20	1200	7	17.91
HGHH92-C12=R281	1993-04-01	4200		17.74
HGHH92-C12=R281	2002-04-19	1800	6	17.74
HHH86-C15=R226	2002-04-19	1800	5	18.56
HGHH92-C17	1993-04-01	4800		17.63
HGHH92-C17	1993-04-02	4500		17.63
HHH86-C18	1993-04-02	4500		17.53
HGHH92-C21	1993-04-01	4200		17.87
HGHH92-C21	2002-04-20	1200	5.5	17.87
HGHH92-C22	2002-04-20	1800	7.5	18.15
HGHH92-C23	1993-03-31	4500		17.22
HGHH92-C23	1993-04-02	4500		17.22
HGHH92-C23	2002-04-19	1200	10	17.22
HGHH92-C23	2002-04-20	1200	9	17.22
HGHH92-C29	2002-04-20	1200	6.5	18.15
HGHH92-C36=R113	2002-04-19	1800	5.5	18.35
HGHH92-C37=R116	2002-04-19	1800	6.5	18.43
HHH86-C38=R123	2002-04-20	1800	6	18.41
HGHH92-C41	2002-04-20	1800	6	18.59
HGHH92-C44	2002-04-19	1800	4	18.69
HGHH92-C44	2002-04-19	1800	5	18.69
HCH99-2	2002-04-20	1200	4	18.21
HCH99-15	2002-04-19	1200	6	17.56
HCH99-16	2002-04-20	1800	3.5	18.45
HCH99-18	2002-04-19	1200	8	17.07
HCH99-21	2002-04-20	1208	3.5	18.41
R115	2002-04-20	2700	2	19.44
R122	2002-04-19	1800	7	18.09
R223	2002-04-19	1800	5	18.77
R261	2002-04-19	1800	5.5	18.20

The data reduction was done both using the *echelle* package in IRAF (Willmarth & Barnes 1994) and the MIDAS based ESO-UVES pipeline (Ballester et al. 2000), where we have taken care to assign the wavelength calibration spectrum taken after each target spectrum in order to have the highest preci-

**Table 2.** Template stars observed with UVES during the 2002 run. The columns list: (1) identifier, (2) number of observed spectra, (3) spectral type, (4) apparent V band magnitude from the literature, (5) metallicity from the literature, (6) radial velocity from the literature, (7) measured radial velocity, (8) reference for catalogue value of radial velocity, and average  $\sigma_{CCF}$  measured from cross-correlation with all the other stars for (9) lower CCD, and (10) upper CCD (see Eq. 1 for the definition of  $\sigma_{CCF}$ ).

(1) ID	(2) N	(3) Sp. Typ	(4) V (mag)	(5) [Fe/H]	(6) V <sub>R</sub> (cat)	(7) V <sub>R</sub> (UVES)	(8) Ref.	(9) $\sigma'_{CCF}$	(10) $\sigma''_{CCF}$
HD 103295	2	G5/G6 III	9.60	-1.01	3.0 ± 0.3	-2.6 ± 0.3	N04	12.2 ± 0.3	11.5 ± 0.2
HD 107328	2	K1 III	5.00	-0.48	36.40 ± 0.01	36.4 ± 0.1	F05	12.4 ± 0.2	11.7 ± 0.1
HD 146051	3	M1 III	2.74	+0.32	-19.6 ± 0.3	-20.1 ± 0.3	COR	12.9 ± 0.2	12.0 ± 0.1
HD 150798	1	K2 II-III	1.92	-0.06	-3.0 ± 0.3	-3.0 ± 0.1	COR	13.0 ± 0.2	12.2 ± 0.1
HD 161096	1	K2 III	2.77		-12.53 ± 0.01	-12.5 ± 0.1	F05	12.6 ± 0.2	11.8 ± 0.1
HD 165195	1	K3 III	7.34	-2.24	-0.3 ± 0.2	-0.5 ± 0.2	F05	12.7 ± 0.5	11.9 ± 0.2
HD 168454	1	K3 III	2.71		-20.4 ± 0.3	-20.5 ± 0.1	COR	12.7 ± 0.2	11.9 ± 0.1
HD 171391	1	G8 III	5.13	-0.07	7.4 ± 0.2	7.3 ± 0.2	COR	12.5 ± 0.2	11.7 ± 0.1
HD 196983	2	K2 III	9.08		-9.1 ± 0.3	-9.1 ± 0.2	COR	12.6 ± 0.2	11.7 ± 0.1
HD 203638	3	K0 III	5.37	+0.30	22.1 ± 0.2	22.1 ± 0.1	COR	12.6 ± 0.2	11.7 ± 0.1
HD 33771	2	G0 III	9.50	-2.56	-13.6 ± 0.4	-13.6 ± 0.2	D97	12.4 ± 0.5	11.7 ± 0.3
HD 66141	3	K2 III	4.40	-0.36	71.57 ± 0.01	71.5 ± 0.4	F05	12.4 ± 0.2	11.6 ± 0.1
HD 81797	2	K3 III	1.99	-0.12	-4.7 ± 0.3	-4.7 ± 0.3	COR	12.7 ± 0.2	11.9 ± 0.1
HD 83212	1	G8 IIIw	8.34	-1.51	108.7 ± 0.3	109.1 ± 0.1	D97	12.4 ± 0.3	11.7 ± 0.2
HD 93529	1	G6/G8w	9.31	-1.56	145.4 ± 0.3	144.9 ± 0.3	D97	12.2 ± 0.4	11.5 ± 0.2
NGC 2447-s28	1	G8/K0 III	10.15	+0.10	21.2 ± 0.1	21.8 ± 0.1	D97	12.4 ± 0.2	11.7 ± 0.1
NGC 2447-s4	1	G8/K0 III	9.85	+0.10	23.2 ± 0.2	23.1 ± 0.2	D97	12.4 ± 0.2	11.7 ± 0.1

References: All the radial velocities except those from D97 (Dubath et al. 1997) are compiled from

<http://www.casleo.gov.ar/catalogue/catalogue.html>, which lists references to the sources:

N04 (Nordström et al. 2004); F05 (Famaey et al. 2005);

COR (Udry et al. 1999, see also: <http://obswww.unige.ch/udry/std/stdcor.dat>).

sion in the wavelength calibration. Due to low S/N ratio of the spectra, the MIDAS pipeline was not used in optimal extraction mode. The final spectra were normalized using the *continuum* task in IRAF and the cosmic rays were excised by hand. After some tests to ensure that the pipeline results were giving the same results as manual reductions done within IRAF, we have decided to later use spectra reduced within the MIDAS pipeline because the different echelle orders were combined in one long 1D spectrum per CCD, offering thus the maximum number of lines for cross-correlation.

### 3. Cross-correlation

In order to measure radial velocities and velocity dispersions of all our targets we have used cross-correlation technique (Tonry & Davis 1979). Slightly different implementation of the cross-correlation technique has been adopted for the EMMI and UVES spectra. The comparison of the resulting velocity dispersion measurements for the 5 targets in common between the two datasets is providing a useful check on the results obtained with these two slightly different methods.

EMMI spectra were cross-correlated with a numerical mask specially designed for globular clusters. This has been described in greater detail by Dubath et al. (1990, 1992) and thus we do not repeat it here.

The globular cluster spectra observed with UVES have been cross-correlated with the high signal to noise spectra of template radial velocity stars observed during the same run, using the IRAF task *FXCOR* in the *RV* package. All the spectra were Fourier-filtered prior to cross-correlation, to remove the

residual low frequency features arising from imperfect continuum fitting to the spectra with combined echelle orders. The features at frequencies higher than the intrinsic resolution of the spectrograph were also cut. The peak of the cross-correlation function (CCF) traces the radial velocity, and the width is a function of the velocity dispersion and of the instrumental width. The latter is measured by cross-correlating the template stars spectra with each other. Since we have observed a large number of radial velocity standard stars as well as giant star templates with a range of metallicities, we could check that the template miss-match does not produce spurious results. This is described in detail in the next section.

#### 3.1. Template stars

The measured radial velocities for all the stars observed during the 2002 run with UVES are given in Table 2 in column 7. They were measured by cross-correlating each Fourier-filtered stellar spectrum against each other. The resulting radial velocities for each individual spectrum were averaged and we report here the average radial velocity and standard deviation for each star. In column 6 we list the radial velocity from the literature. These were compiled from Dubath et al. (1997) and the web database of stellar radial velocities (see table footnote). In all but one case the difference between our measured radial velocities from UVES spectra and those from the literature is smaller than 1 km s<sup>-1</sup> and the measurements are consistent with the catalogue values within the errors. Since the stars were observed with a 1.0 arcsec slit and seeing was sometimes as good as 0.6-0.7 arcsec, part of the error in radial velocities may come

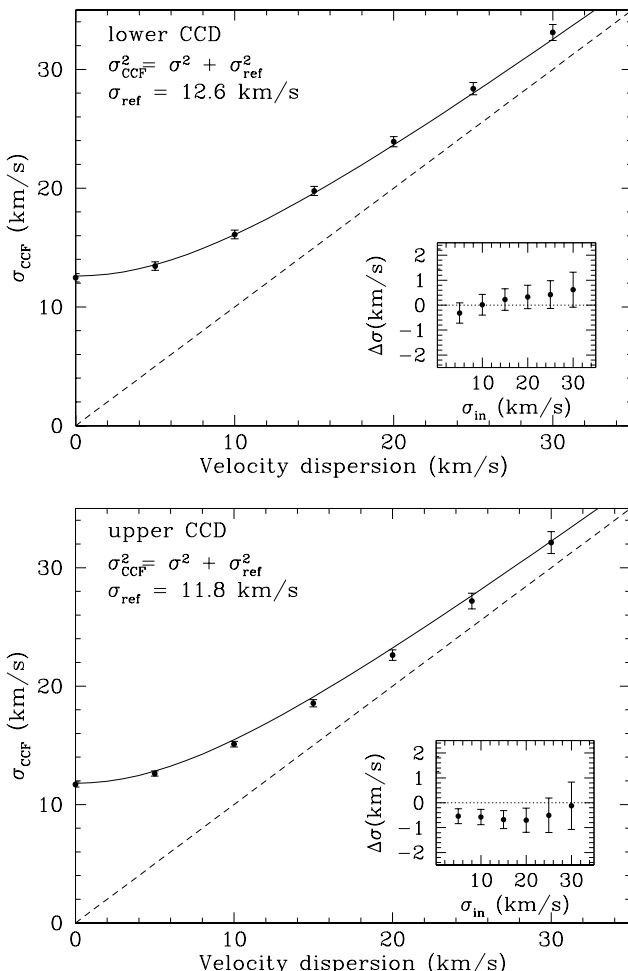


**Fig. 1.** The points with error bars are the average raw velocity dispersion measurements ( $\sigma_{CCF}$ ) obtained from 7 different template stars whose spectra were broadened to simulate the different input velocity dispersion ( $\sigma_{in}$  values). The solid line is from Equ. 1 which is also displayed in each panel. The two diagrams are for the lower and upper CCDs of UVES which have different  $\sigma_{ref}$  values. The inserts show the difference between the obtained and input true velocity dispersion as a function of input velocity dispersion.

from slit centering errors. The star that shows the largest difference, HD 103295, has less certain value of the radial velocity and the quoted error from the literature is evidently underestimated. Leaving HD 103295 out, the average difference between our radial velocity measurements and catalogued values is  $V_R(UVES) - V_R(cat) = 0.07 \pm 0.27 \text{ km s}^{-1}$  indicating that the systematic errors due to slit centering are not significant. For the cross-correlation of stars with cluster spectra we adopt our measured radial velocity for HD 103295, and literature values for all the other stars.

The projected velocity dispersions ( $\sigma$ ) for globular clusters are derived from the broadening of the cluster cross-correlation function (CCF) produced by the Doppler line broadening present in the integrated-light spectra due to the random spatial motion of stars. The raw measurement ( $\sigma_{CCF}$ ) is however

a quadratic sum of the  $\sigma$  and the intrinsic instrumental width ( $\sigma_{ref}$ ) (Dubath et al. 1992):

$$\sigma_{CCF}^2 = \sigma^2 + \sigma_{ref}^2 \quad (1)$$

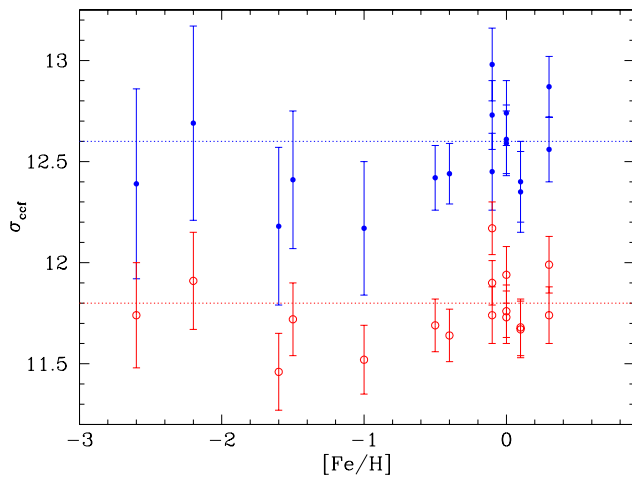
The  $\sigma_{ref}$  value is determined for both UVES CCDs by taking the average value of  $\sigma_{CCF}$  measurements obtained by cross-correlating 18 selected best template stellar spectra, belonging to 13 different stars, with all the other stars. This same set of stars is used in cross-correlation of globular cluster spectra as well as in all the simulations (see below). Since all these stars are late-type giants they are not expected to exhibit line broadening due to rotation. For 3 stars, HD 66141, HD 107328, and HD 161096, de Medeiros & Mayor (1999) provide measurements of rotational velocities which are, 1.1, 1.3, and  $< 1.0 \text{ km s}^{-1}$ , respectively, with uncertainties which are of the same order of magnitude. The fact that for all the stars CCF has similar width (see Table 2) implies that rotation is not a concern. The weighted average of the stellar CCFs are  $12.6 \pm 0.2 \text{ km s}^{-1}$  for the lower and  $11.8 \pm 0.2 \text{ km s}^{-1}$  for the upper CCD. The difference in the instrumental width reflects the different resolution of the two spectral ranges. Excluding from the average HD 150798, the star that shows the widest cross-correlation peak for both spectral ranges, does not change the average value of  $\sigma_{ref}$ .

Figure 1 shows the validity of the Equ. 1 for the lower and upper CCDs of UVES. The solid line is from Equ. 1 and the points represent the average projected velocity dispersion measurements obtained from 7 different template stars whose spectra were broadened by convolving each of them with Gaussians with known sigma ( $\sigma_{in}$ ) of 5, 10, 15, 20, 25 and 30 km s<sup>-1</sup>. The velocity dispersion was then measured on these broadened spectra by convolving them with the 18 selected best template stellar spectra and averaging the resulting velocity dispersions. The smaller inserts in each of the panels in Fig. 1 show the difference between the average measured and input velocity dispersion as a function of the input velocity dispersion, while the main panel displays the averages of the raw measurements ( $\sigma_{CCF}$ ) at each  $\sigma_{in}$  value.

We have carefully selected the regions for cross-correlation, avoiding strong lines such as  $H_\beta$ ,  $H_\alpha$ , sodium region, as well as Mgb region. When we included for example  $H_\alpha$  line, we noticed a strong trend of cross-correlation width as a function of metallicity. In the final selection, this dependence is not present as can be seen from Fig. 2.

In Fig. 3 we tested the dependence of the measured velocity dispersion on S/N of the input spectra. The measured velocity dispersions from the most broadened spectra, with  $\sigma_{in} = 30 \text{ km s}^{-1}$  and with the lowest S/N, appear to be slightly underestimated. However, these have, as expected higher uncertainty and are consistent with the input values within the errors.

The observations of radial velocity standards were also secured during the 1993 EMMI run and were used to check that the CCF has Gaussian shape and that its width does not depend on the stellar metallicity (see also Dubath et al. 1990, 1992). The average sigma of the stellar CCFs, derived from 10 measurements of K-giant radial velocity standard stars observed



**Fig. 2.** Width of the cross-correlation function for stars is plotted as a function of metallicity. The measurements on the lower CCD are plotted with filled and on the upper CCD with open circles.

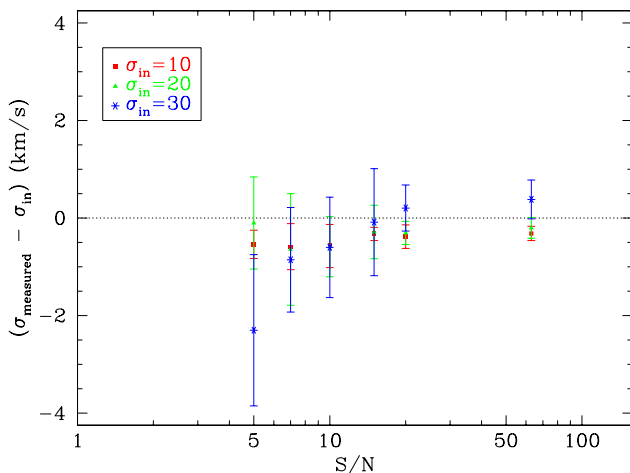


**Fig. 3.** Difference between the measured and simulated velocity dispersion as a function of S/N of the spectra. These simulations are based on randomly selected 7 template stars whose spectra were broadened by convolving them with Gaussians with widths of 10, 20, and 30  $\text{km s}^{-1}$  and had S/N degraded to simulate noisy spectra, more similar to globular cluster targets. (See the electronic edition of the journal for the colour version of this figure.)

during that same run, is  $6.2 \pm 0.3 \text{ km s}^{-1}$ , where  $0.3 \text{ km s}^{-1}$  is the standard deviation around the mean.

### 3.2. Cluster radial velocities and velocity dispersions

The initial estimate of the radial velocity for all the clusters was obtained by fitting the  $H_{\alpha}$  line. In all but one cluster spectrum the line was well defined and could be fitted with a Gaussian profile using *splot* task in IRAF. Then the precise radial velocities and velocity dispersions were measured using *fxcor* IRAF task.

**Table 3.** Radial velocity measurements for globular clusters observed with EMMI and UVES are listed in column (4). For clusters with multiple observations the reported value is a weighted average of velocities measured from individual spectra and the combined spectrum. The last column is the radial velocity from Peng et al. (2004a) catalogue.  $B - V$  and  $V - I$  colours were taken from Peng et al. (2004a) when available, otherwise from original discovery papers. They have been dereddened assuming only foreground reddening of  $E(B - V) = 0.11$  (Schlegel et al. 1998), except for clusters observed by Holland et al. (1999, HCH99) which have individual reddening from that work. Reddening assumed for HGH92-C23 is 0.31, derived from strong interstellar NaD absorption lines (see text for more details).

(1) ID	(2) ( $B - V$ ) <sub>0</sub> (mag)	(3) ( $V - I$ ) <sub>0</sub> (mag)	(4) $V_R$ ( $\text{km s}^{-1}$ )	(5) $V_R(\text{P04})$ ( $\text{km s}^{-1}$ )
HGH92-C1	...	...	$642.4 \pm 1.0$	$633 \pm 11$
VHH81-C3	0.91	1.08	$561.8 \pm 1.6$	$528 \pm 65$
VHH81-C5	0.70	0.82	$556.6 \pm 2.5$	$556 \pm 19$
HGH92-C6	0.85	1.00	$854.5 \pm 1.8$	$828 \pm 65$
HGH92-C7	0.75	0.91	$594.9 \pm 0.5$	$617 \pm 10$
HGH92-C11	0.94	1.12	$753.0 \pm 0.4$	$755 \pm 11$
HGH92-C12=R281	...	...	$440.4 \pm 0.3$	$443 \pm 9$
HHH86-C15=R226	0.89	1.03	$644.3 \pm 0.4$	$638 \pm 18$
HGH92-C17	0.77	0.88	$781.3 \pm 1.8$	$783 \pm 12$
HHH86-C18	0.78	0.92	$479.8 \pm 2.1$	$494 \pm 65$
HGH92-C21	0.78	0.93	$461.3 \pm 2.1$	$465 \pm 7$
HGH92-C22	0.79	0.91	$578.4 \pm 0.3$	$565 \pm 13$
HGH92-C23	0.76	0.78	$673.7 \pm 0.9$	$677 \pm 9$
HGH92-C29	0.89	1.08	$726.1 \pm 0.4$	$733 \pm 10$
HGH92-C36=R113	0.73	0.85	$702.7 \pm 1.1$	$680 \pm 12$
HGH92-C37=R116	0.84	0.99	$611.7 \pm 0.3$	$630 \pm 14$
HHH86-C38=R123	0.78	0.91	$405.1 \pm 0.7$	$418 \pm 12$
HGH92-C41	0.89	1.09	$363.0 \pm 0.2$	$370 \pm 15$
HGH92-C44	0.69	0.85	$504.8 \pm 0.8$	$538 \pm 56$
HCH99-2	0.74	0.84	$300.4 \pm 2.0$	$299 \pm 18$
HCH99-15	...	1.06	$518.6 \pm 0.7$	...
HCH99-16	...	0.79	$458.2 \pm 2.3$	$454 \pm 44$
HCH99-18	0.89	0.89	$455.0 \pm 0.5$	$447 \pm 14$
HCH99-21	...	0.78	$662.9 \pm 1.5$	$669 \pm 22$
R122	...	...	$588.4 \pm 1.5$	...
R223	0.80	0.95	$775.7 \pm 0.6$	$572 \pm 56$
R261	0.83	0.99	$614.8 \pm 3.9$	$613 \pm 12$

Radial velocity measurements for all the clusters are listed in Table 3. After the identifier, de-reddened  $(B - V)_0$  and  $(V - I)_0$  colours of the targets are given. The radial velocities measured from our spectra are in column 4, and the velocities from the catalogue of Peng et al. (2004a) are shown for comparison in the last column. For clusters with both EMMI and UVES spectra the radial velocities reported are weighted averages of both measurements. The individual radial velocity and velocity dispersion measurements for clusters with multiple observations are reported in Table 4. We note that the values listed as “combined” are not the averages of individual measurements, but rather the measurements of the radial velocity and velocity dispersion from the combined UVES spectra, constructed by aver-

**Table 4.** Radial velocities and velocity dispersions measured on individual spectra for cluster targets with multiple observations. The values listed as “combined” are not the averages of individual measurements, but rather the measurements from the combined UVES spectra, constructed by averaging individual exposures.

(1) ID	(2) $V_R$ km s $^{-1}$	(3) $\sigma$ km s $^{-1}$	(4) Inst.
<b>HGHH92-c1</b>			
combined	$638.0 \pm 5.6$	$13.1 \pm 2.3$	UVES
A	$639.2 \pm 3.8$	$11.9 \pm 1.2$	UVES
B	$643.6 \pm 1.8$	$14.1 \pm 1.4$	UVES
1	$642.5 \pm 2.1$	$14.1 \pm 1.7$	EMMI
<b>HGHH92-c6</b>			
1	$857.3 \pm 2.1$	$19.5 \pm 1.7$	EMMI
2	$847.9 \pm 3.2$	$24.5 \pm 3.0$	EMMI
<b>HGHH92-c7</b>			
combined	$592.9 \pm 1.4$	$24.1 \pm 1.6$	UVES
A	$594.7 \pm 0.9$	$21.1 \pm 0.1$	UVES
B	$595.8 \pm 0.7$	$24.2 \pm 1.4$	UVES
C	$595.1 \pm 0.9$	$24.7 \pm 1.4$	UVES
1	$590.9 \pm 2.3$	$22.2 \pm 1.9$	EMMI
2	$593.6 \pm 2.1$	$17.6 \pm 1.8$	EMMI
<b>HGHH92-c11</b>			
combined	$753.1 \pm 0.5$	$18.4 \pm 1.0$	UVES
A	$752.4 \pm 1.2$	$18.2 \pm 2.0$	UVES
B	$753.1 \pm 0.8$	$19.4 \pm 0.4$	UVES
<b>HGHH92-c12 = R281</b>			
A	$440.4 \pm 0.3$	$13.1 \pm 0.5$	UVES
1	$439.2 \pm 1.5$	$13.4 \pm 0.9$	EMMI
<b>HGHH92-c17</b>			
1	$777.8 \pm 2.8$	$16.5 \pm 2.5$	EMMI
2	$783.7 \pm 2.3$	$23.7 \pm 2.0$	EMMI
<b>HGHH92-c21</b>			
A	$460.2 \pm 1.2$	$19.0 \pm 0.1$	UVES
1	$465.5 \pm 2.4$	$16.3 \pm 2.1$	EMMI
<b>HGHH92-c23</b>			
combined	$671.4 \pm 1.3$	$30.9 \pm 1.5$	UVES
A	$674.5 \pm 1.7$	$30.5 \pm 0.2$	UVES
B	$675.8 \pm 1.5$	$28.6 \pm 2.1$	UVES
1	$673.4 \pm 2.1$	$26.3 \pm 1.8$	EMMI
2	$675.8 \pm 2.9$	$25.8 \pm 2.7$	EMMI
<b>HGHH92-c44</b>			
combined	$504.2 \pm 1.1$	$8.4 \pm 3.4$	UVES
A	$505 \pm 18$	$9.8 \pm 2.2$	UVES
B	$505.4 \pm 1.1$	$14.6 \pm 1.2$	UVES

aging individual exposures. These spectra have slightly higher S/N and the agreement between the values obtained from the individual and these combined spectra indicates the absence of significant systematic errors (Fig. 3).

Dubath et al. (1997) have made detailed numerical simulations in order to understand and estimate the statistical errors on their radial velocity and projected velocity dispersion  $\sigma_p$  measurements obtained by applying a cross-correlation technique to integrated-light spectra. They show that statistical errors, which can be very important for integrated-light measurements of Galactic (nearby) globular clusters, because of the

dominance of a few bright stars, are negligible in the present case where sampling problems are not present, thanks to the larger distances of our targets. An integrated light spectrum of an NGC 5128 globular cluster is well approximated by the convolution of the spectrum of a typical globular cluster star with the projected velocity distribution. The influence of binary stars is negligible (e.g. Olszewski et al. 1996, for dSph galaxies).

The measurements of velocity dispersions for all the clusters are given in Table 5. In the first column is the identifier, then we list velocity dispersion measured on UVES spectra. In the third column the velocity dispersions measured on EMMI spectra are given, while in the last column the results from Martini & Ho (2004) are shown for comparison.

In Fig. 4 we plot the spectrum of the highest S/N cluster, the combined three 20 min exposures of HGHH92-C7, centered on some of the characteristic absorption lines. Overplotted are broadened spectra of HD 103295 made by convolving with Gaussians of 5 (red), 15 (blue) and 25 km s $^{-1}$  (green). The best fitting template is the one broadened to 25 km s $^{-1}$  in agreement with  $24.1 \pm 1.6$  km s $^{-1}$  obtained by cross-correlation (Table 4). The differences between the template broadened with 25 km s $^{-1}$  and the cluster spectra are shown below the spectra in each panel. The narrow lines at 5890.0 and 5895.9 Å, cannot be fitted by the broadened stellar templates. This is expected, because they are resonance lines (Na D1 and Na D2) due to interstellar ions of NaI. The equivalent width of these lines can be used to constrain the interstellar extinction towards each globular cluster (Munari & Zwitter 1997). The equivalent width of Na D1 line in this spectrum implies  $E(B - V) \simeq 0.07$  mag, somewhat lower than the average reddening of 0.11 mag in the line of sight of NGC 5128 from Schlegel et al. (1998) maps. However, we note that both our measurement and the calibration have considerable uncertainty and that the error on the reddening is probably of the same size as the derived value.

In Fig. 5 we plot cross-correlation functions for all the clusters. In each panel, next to the cluster name, the velocity dispersion is given in parenthesis. The x-axis scale has been corrected for the relative velocity shift between the template star and the cluster so that the peak of the CCFs correspond to the heliocentric velocity of each cluster. All the CCFs show a single well defined Gaussian peak, except for R122, which has additional peaks at velocities 59 and at 114 km s $^{-1}$ . We have inspected the through-slit image taken at the start of the exposure as well as deep V-band images taken with FORS 1 under excellent seeing conditions, but there is no sign of a spatially resolved blend at this position. The two additional peaks at the above given velocities are present when cross-correlating the cluster spectrum with all the template stars and the height of these peaks is comparable, and sometimes larger than that corresponding to a velocity plausible for a cluster in NGC 5128. We note that the spectrum of this object also displays additional absorption features. We do not have any explanation for this, other than an unfortunate spatially unresolved blend with foreground MW stars, which is not uncommon given the low Galactic latitude ( $b = +19.4^\circ$ ) of NGC5128.

To calculate the mean and sigma of the velocity dispersion for each spectrum, we first calculate the straight mean and standard deviation of the 18 independent measurements, each ob-

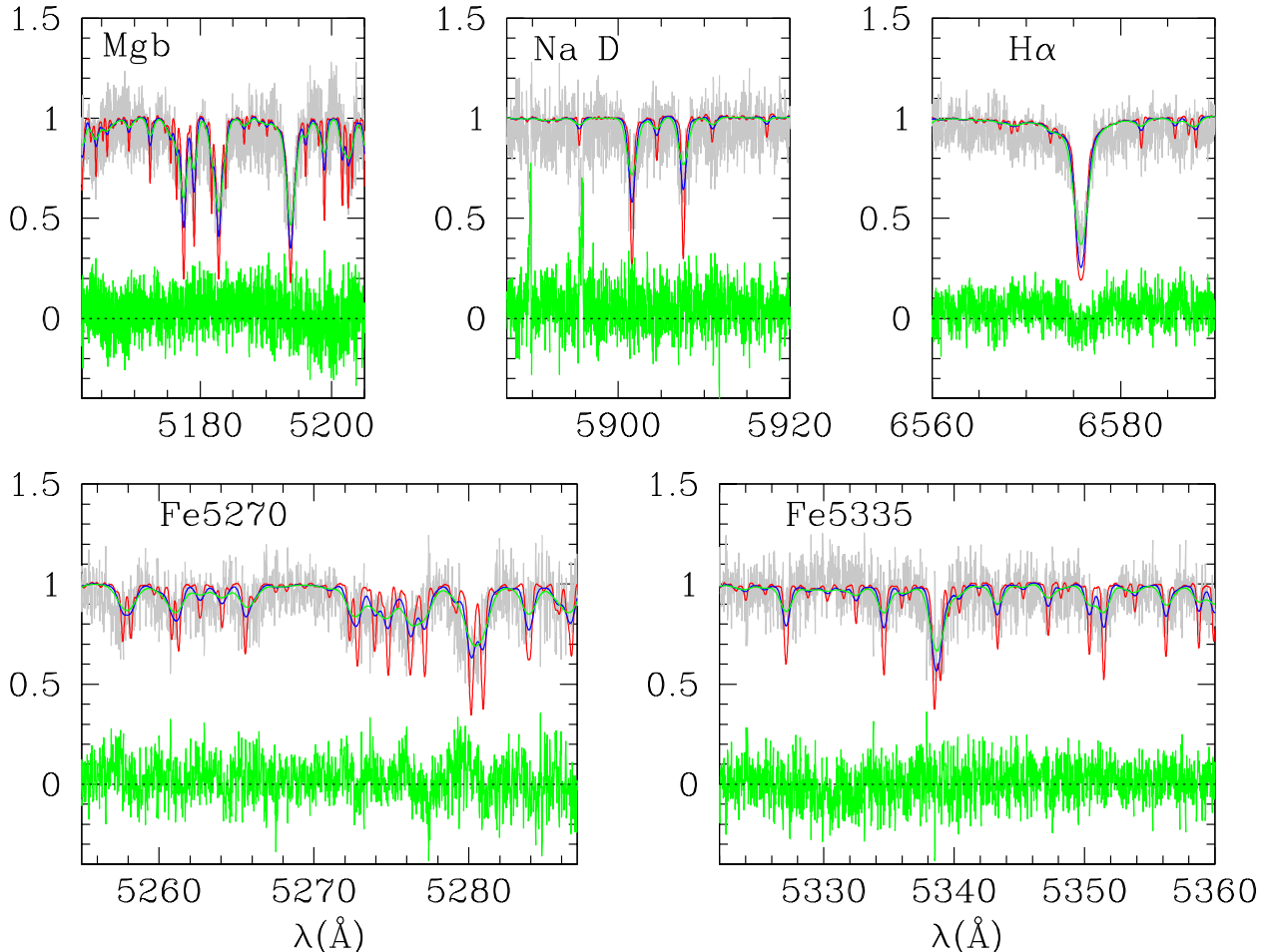


**Fig. 4.** The spectrum of HGHH92-C7 is plotted in gray showing the spectral regions around some of the prominent absorption line features: Mg b, Na D and H $\alpha$  in the upper panel and Fe 5270 and Fe 5335 features in the lower panel. Overplotted are spectra of HD 103295 star broadened to simulate velocity dispersion of 5 (red line), 15 (blue) and 25 km s $^{-1}$  (green). The best fitting template is the one widened by 25 km s $^{-1}$  in agreement with  $24.1 \pm 1.6$  km s $^{-1}$  obtained by cross-correlation (Table 4). The differences (template-GC) are shown at the bottom of each panel demonstrating the goodness of the fit for the template broadened with  $\sigma = 25$  km s $^{-1}$ . (See the electronic edition of the journal for the colour version of this figure.)

tained by cross-correlating the cluster spectrum with a different template star. The error is the quadratic sum of the standard deviation and the uncertainty in the calibration of the instrumental width for the CCF. This is done separately for the upper and lower UVES CCD. We combine the two averaged velocity dispersion measurements through the weighted mean. Since the two chips have slightly different resolution and the calibration of the  $\sigma_{ref}$  is independently made, the uncertainty in the mean is calculated with the average variance of the data using the following expression (Bevington 1969):

$$\sigma_\mu = \sqrt{\frac{\sum_i [w_i(x_i - \mu)^2]}{(N - 1) \sum_i w_i}} \quad (2)$$

where  $w_i = 1/\sigma_i^2$  is the usual definition of weights and  $\mu$  is the weighted mean of the  $x_i$  measurements from the two chips.

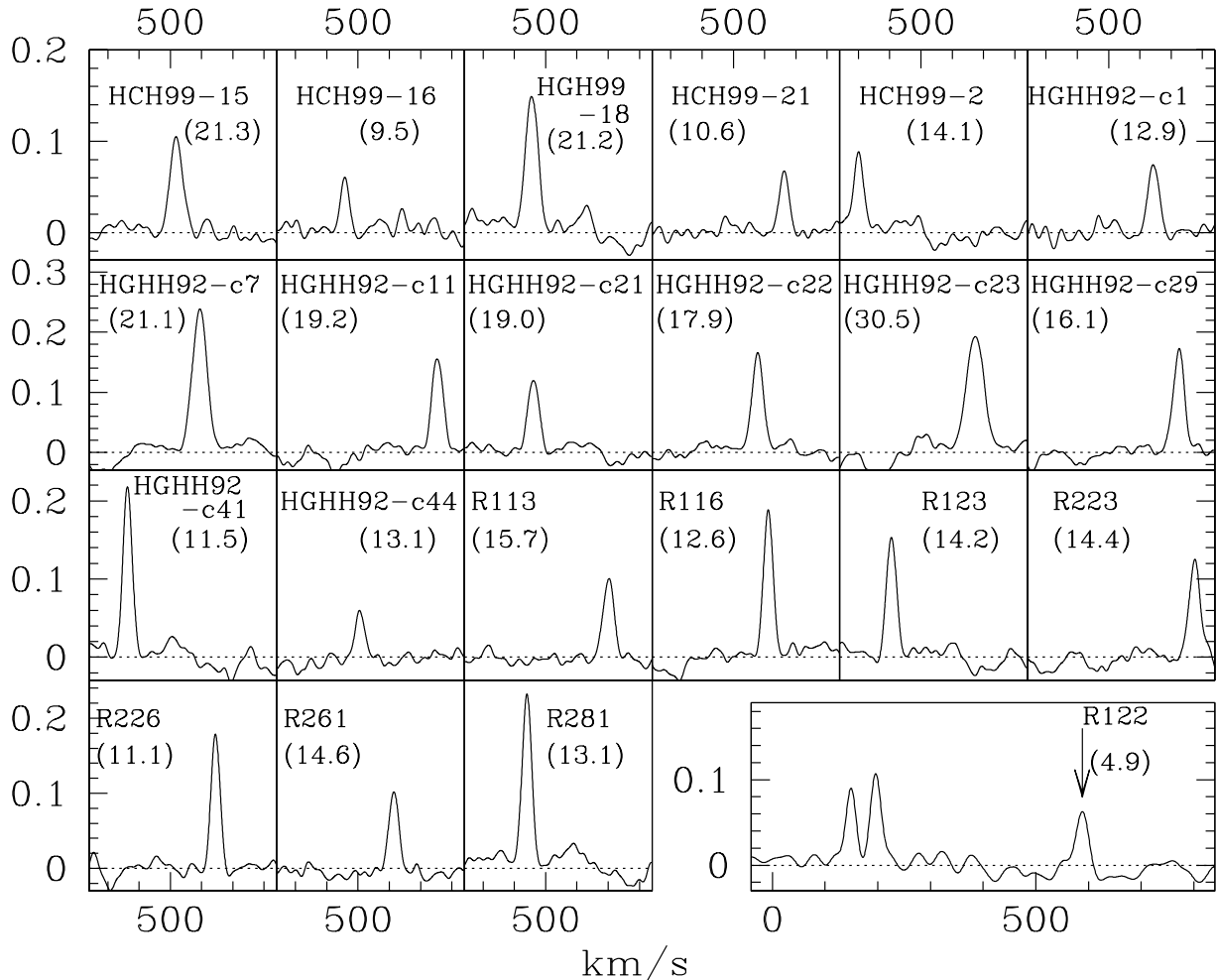
For clusters with multiple observations, the measurements of velocity dispersion from individual spectra are given in

Table 4, while in Table 5 we list the weighted average of the velocity dispersion from all the measurements on spectra taken with the given instrument. In particular the uncertainty in the mean is calculated according to (Bevington 1969):

$$\sigma_\mu = \sqrt{\frac{1}{\sum_i w_i}} \quad (3)$$

### 3.2.1. Comparison with previous measurements

In the upper panel of Fig. 6 we compare our radial velocity measurements with those of Peng et al. (2004a, filled triangles). The average difference is  $8 \pm 43$  km s $^{-1}$ . Due to high resolution and the wide wavelength coverage the errors in radial velocities of our spectra are significantly smaller in spite of their relatively low S/N. The agreement with the previously published measurements is excellent.



**Fig. 5.** The CCFs for all the clusters observed with UVES. The derived velocity dispersion is given in the parenthesis next to the name of each cluster. The x-axis scale has been corrected for the relative velocity shift between the template star and the cluster so that the peak of the CCFs correspond to the heliocentric velocity of the cluster. The x-axis displays one tick for every 100  $\text{km s}^{-1}$ . All the CCFs show a single well defined Gaussian peak, except for that of R122, which has additional peaks at velocities 59 and at 114  $\text{km s}^{-1}$  due to contamination by Galactic foreground stars.

The comparison between the velocity dispersions for the clusters in common with Martini & Ho (2004) work is shown in the lower panel of Fig. 6. The average difference between our velocity dispersions from UVES spectra and those of Martini & Ho (2004, asterisks) is  $0.14 \pm 1.93 \text{ km s}^{-1}$ , while there is a slightly larger difference, amounting to  $2.6 \pm 3.3 \text{ km s}^{-1}$ , between the results obtained by these authors and our velocity dispersions obtained from EMMI spectra (open squares).

For the five clusters in common between our UVES and EMMI datasets, the average difference is  $-0.4 \pm 3.0 \text{ km s}^{-1}$  for radial velocities and  $1.4 \pm 2.3 \text{ km s}^{-1}$  for velocity dispersions. There is no trend with cluster brightness neither for radial velocity, nor for velocity dispersion residuals.

#### 4. Globular cluster structural parameters

Holland et al. (1999) published the measurements of structural parameters for 21 globular cluster candidates in the inner part

of Cen A, based on WFPC2 images from the Hubble Space Telescope (HST). Harris et al. (2002) have used HST STIS unfiltered images to increase the number of clusters with measured structural parameters to 43 in this galaxy. Most of the clusters in our sample have the structural parameters available from these two works. However, for 5 clusters observed with EMMI and 8 clusters observed with UVES such data do not exist in the literature.

The globular cluster candidates selected for the spectroscopic observations from the list of Rejkuba (2001) have, however, images taken with FORS1 imaging spectrograph at the ESO VLT under superb seeing conditions. We have thus used these images to derive the structural parameters for 8 clusters in our sample. Only one of them, R116 which is the same as HGH92-C37, has previously measured parameters from HST imaging. The comparison between the derived parameters from the ground and the space data for this cluster (Table 6) shows good agreement (but in the further analysis we use the more accurate results from the HST data for this cluster), and lends

**Table 6.** Globular cluster structural parameters, projected galactocentric distances, absolute magnitudes, masses, and mass-to-light measurements. The columns are: (1) ID, (2) core radius ( $r_c$ ), (3) projected two-dimensional effective (half-light) radius ( $r_e$ ), (4) three-dimensional half-mass radius ( $r_h$ ), (5) concentration ( $c = \log r_t/r_c$ ), (6) ellipticity ( $\epsilon$ ), (7) projected galactocentric distance ( $R_{gc}$ ), (8) absolute  $V$  magnitude, (9) virial mass ( $M_{vir}$ ) in  $10^6 \text{ M}_\odot$ , and (10)  $M/L_V$ . In the last column we list the source for the structural parameters.

(1) ID	(2) $r_c$ (pc)	(3) $r_e$ (pc)	(4) $r_h$ (pc)	(5) $c$ ( $\log r_t/r_c$ )	(6) $\epsilon$	(7) $R_{gc}$ (kpc)	(8) $M_V$ (mag)	(9) $M_{vir}$ ( $10^6 \text{ M}_\odot$ )	(10) $M/L_V$ ( $\text{M}_\odot/\text{L}_\odot$ )	(11) Ref.
HGHH92-C7	$1.4 \pm 0.1$	$7.5 \pm 0.1$	$10.0 \pm 0.2$	1.83	0.13	9.3	-11.09	$7.8^{+0.7}_{-1.9}$	$3.3^{+0.8}_{-1.1}$	2
HGHH92-C11	$1.3 \pm 0.1$	$7.8 \pm 0.1$	$10.4 \pm 0.2$	1.88	0.26	6.7	-10.35	$6.7^{+0.6}_{-1.6}$	$5.7^{+1.4}_{-1.9}$	2
HGHH92-C12=R281	$1.2 \pm 0.2$	$10.8 \pm 1.4$	$14.4 \pm 1.9$	2.4	0.20	11.4	-10.52	$4.3^{+0.7}_{-1.3}$	$3.1^{+0.9}_{-1.2}$	1
HHH86-C15=R226	$1.2 \pm 0.2$	$5.3 \pm 0.7$	$7.1 \pm 0.9$	1.9	0.05	11.9	-9.70	$1.5^{+0.2}_{-0.5}$	$2.3^{+0.6}_{-0.9}$	1
HGHH92-C17	$2.3 \pm 0.1$	$5.7 \pm 0.1$	$7.6 \pm 0.2$	1.43	0.07	6.2	-10.63	$5.8^{+0.5}_{-1.4}$	$3.8^{+0.9}_{-1.3}$	2
HGHH92-C21	$1.2 \pm 0.1$	$7.0 \pm 0.1$	$9.3 \pm 0.2$	1.86	0.33	7.3	-10.39	$5.8^{+0.5}_{-1.4}$	$4.8^{+1.1}_{-1.6}$	2
HGHH92-C22	$1.1 \pm 0.1$	$3.8 \pm 0.1$	$5.1 \pm 0.2$	1.62	0.09	5.8	-10.11	$2.8^{+0.3}_{-0.7}$	$3.0^{+0.7}_{-1.0}$	2
HGHH92-C23	$0.9 \pm 0.1$	$3.3 \pm 0.1$	$4.4 \pm 0.2$	1.67	0.14	5.8	-11.66	$7.2^{+0.7}_{-1.8}$	$1.8^{+0.5}_{-0.6}$	2
HGHH92-C29	$1.2 \pm 0.1$	$6.9 \pm 0.1$	$9.2 \pm 0.2$	1.87	0.11	21.2	-10.11	$4.1^{+0.4}_{-1.0}$	$4.4^{+1.0}_{-1.4}$	2
HGHH92-C36=R113	$0.7 \pm 0.3$	$3.6 \pm 0.3$	$4.8 \pm 0.4$	2.0	0.32:	13.1	-9.91	$2.0^{+0.3}_{-0.6}$	$2.6^{+0.6}_{-0.9}$	1
HGHH92-C37=R116	$0.6 \pm 0.1$	$3.3 \pm 0.1$	$4.4 \pm 0.2$	1.87	0.02	12.1	-9.83	$1.2^{+0.1}_{-0.3}$	$1.7^{+0.4}_{-0.6}$	2
HGHH92-C37=R116	$0.7 \pm 0.2$	$2.9 \pm 0.3$	$3.9 \pm 0.4$	1.9	0.21:	12.1	-9.83	$1.1^{+0.1}_{-0.3}$	$1.5^{+0.4}_{-0.6}$	1
HHH86-C38=R123	$0.5 \pm 0.2$	$2.8 \pm 0.2$	$3.7 \pm 0.3$	2.2	0.10	14.0	-9.85	$1.3^{+0.2}_{-0.4}$	$1.8^{+0.4}_{-0.6}$	1
HGHH92-C41	$0.8 \pm 0.1$	$4.5 \pm 0.1$	$6.0 \pm 0.2$	1.87	0.05	23.4	-9.67	$1.4^{+0.1}_{-0.3}$	$2.2^{+0.5}_{-0.7}$	2
HGHH92-C44	$1.3 \pm 0.1$	$5.7 \pm 0.1$	$7.6 \pm 0.2$	1.70	0.06	20.4	-9.57	$2.3^{+0.2}_{-0.6}$	$3.9^{+0.9}_{-1.3}$	2
HCH99-2	$1.0 \pm 0.1$	$11.4 \pm 1.1$	$15.2 \pm 1.5$	1.5	0.08	2.6	-10.33	$5.3^{+0.7}_{-1.5}$	$4.5^{+1.2}_{-1.8}$	3
HCH99-15	$1.6 \pm 0.1$	$5.9 \pm 0.2$	$7.8 \pm 0.3$	1.0	0.08	1.2	-10.82	$6.2^{+0.6}_{-1.5}$	$3.4^{+0.8}_{-1.1}$	3
HCH99-16	$0.8 \pm 0.2$	$12.1 \pm 0.6$	$16.1 \pm 0.8$	1.6	0.30	1.8	-10.08	$2.5^{+0.3}_{-0.6}$	$2.8^{+0.7}_{-0.9}$	3
HCH99-18	$1.2 \pm 0.0$	$13.7 \pm 0.3$	$18.3 \pm 0.3$	1.5	0.03	1.5	-11.38	$14.3^{+1.3}_{-3.5}$	$4.7^{+1.2}_{-1.6}$	3
HCH99-21	$2.6 \pm 1.1$	$7.1 \pm 2.7$	$9.5 \pm 3.6$	0.8	0.02	3.0	-10.28	$1.9^{+0.7}_{-1.0}$	$1.7^{+0.7}_{-1.0}$	3
R122	$0.6 \pm 0.3$	$2.2 \pm 0.4$	$2.9 \pm 0.4$	1.7	0.39:	12.0	-10.17	$0.12^{+0.02}_{-0.04} :$	$0.12^{+0.03}_{-0.04} :$	1
R223	$0.5 \pm 0.4$	$2.6 \pm 0.3$	$3.5 \pm 0.4$	2.0	0.06	6.6	-9.49	$1.3^{+0.2}_{-0.4}$	$2.3^{+0.6}_{-0.9}$	1
R261	$0.4 \pm 0.2$	$1.9 \pm 0.4$	$2.6 \pm 0.5$	2.0	0.17	8.2	-10.06	$1.0^{+0.2}_{-0.3}$	$1.1^{+0.3}_{-0.4}$	1

References: 1: FORS1 data (this work); 2: Harris et al. (2002); 3: Holland et al. (1999).

confidence in the results from the King-profile fitting from these ground based images. Measurements of the profiles of the other 7 clusters observed with FORS1 are published here for the first time.

The full description of the FORS1 dataset used here is given by Rejkuba (2001) and we will thus not repeat it. The most relevant parameters for the profile measurements are the seeing and the pixel scale. The seeing measured on the deep combined U-band images was  $0''.52$  and  $0''.55$  for the field 1 and 2, respectively. The V-band images had seeing of  $0''.54$  and  $0''.46$ , but unfortunately these bright globular clusters had saturated cores in V-band. The pixel scale is  $0''.2/\text{pix}$ .

To measure the structural parameters we have used ISHAPE programme (Larsen 1999, 2001) which models the light distribution of the cluster by convolving the assumed analytical model of the intrinsic luminosity profile of the cluster with the stellar PSF. The convolved model image is then subtracted from the observed image of the cluster and, via a  $\chi^2$  minimization algorithm, ISHAPE returns the best fitting model parameters and also produces the residual image which can be examined in detail.

In particular for the modeling of these globular clusters the King profile (King 1962) was assumed. In this model the core and tidal radii of a cluster are defined by the concentration parameter  $c = \log r_t/r_c$ . The implementation of the concentration

parameter in ISHAPE is slightly different with its definition in the linear scale ( $C = r_t/r_c$ ). We shall call this ISHAPE concentration parameter  $C$  in order to avoid confusion. Since  $C$  is the most uncertain of the fitted parameters in ISHAPE (Larsen 2001) and its best fitting value depends on the initial guesses, we have run a series of measurements with the fixed  $C$  of 5, 15, 30, 50, 75, 100, 150, 200, 250 and 300. In all cases the best fit (the lowest  $\chi^2$ ) shows the smallest amount of residuals in the subtracted image.

Table 6 lists the structural parameters for all our targets, except for the 6 clusters for which no high enough resolution optical images were available. In column 1 we list the cluster ID and its core radius ( $r_c$ ) in column 2. Columns 3 and 4 report the projected two-dimensional half-light (effective) radius ( $r_e$ ) and the three-dimensional half-mass radius ( $r_h$ ), respectively. Concentration parameter ( $c$ ) is listed in column 5 and ellipticity in column 6. In all cases cluster radii are given in parsecs assuming the distance of  $3.84 \text{ Mpc}$  (Rejkuba 2004). This is the same distance used in the work of Martini & Ho (2004) allowing a straight-forward comparison. We note that using the shorter distance of Ferrarese et al. (2006), the radii would be 11% smaller.

Out of 6 clusters which have their structural parameters determined here for the first time, three have ellipticities larger than 0.1. We note however that significantly larger ellipticity

**Table 5.** Velocity dispersion measurements for the clusters observed with UVES are listed in column 2 and for those observed with EMMI in column 3. For clusters with several observations the reported value is the weighted average of individual measurements (for each instrument separately). All the measurements from individual spectra are reported in Table 4. For comparison in column 4 we list velocity dispersion measurements from Martini & Ho (2004).

(1) ID	(2) $\sigma$ (UVES) (km s <sup>-1</sup> )	(3) $\sigma$ (EMMI) (km s <sup>-1</sup> )	(4) $\sigma$ (MH04) (km s <sup>-1</sup> )
HGHH92-C1	$12.9 \pm 0.8$	$14.1 \pm 1.7$	...
VHH81-C3	...	$16.1 \pm 1.1$	...
VHH81-C5	...	$15.8 \pm 2.2$	...
HGHH92-C6	...	$20.7 \pm 1.5$	...
HGHH92-C7	$21.1 \pm 0.1$	$19.8 \pm 1.3$	$22.4 \pm 2.1$
HGHH92-C11	$19.2 \pm 0.4$	...	$17.7 \pm 1.9$
HGHH92-C12=R281	$13.1 \pm 0.5$	$13.4 \pm 0.9$	...
HHH86-C15=R226	$11.1 \pm 0.7$	...	...
HGHH92-C17	...	$20.9 \pm 1.6$	$18.9 \pm 2.0$
HGHH92-C18	...	$15.3 \pm 1.8$	...
HGHH92-C21	$19.0 \pm 0.1$	$16.3 \pm 2.1$	$20.8 \pm 1.9$
HGHH92-C22	$17.9 \pm 0.1$	...	$19.1 \pm 2.0$
HGHH92-C23	$30.5 \pm 0.2$	$26.1 \pm 1.5$	$31.4 \pm 2.6$
HGHH92-C29	$16.1 \pm 0.8$	...	$16.1 \pm 2.1$
HGHH92-C36=R113	$15.7 \pm 1.9$	...	...
HGHH92-C37=R116	$12.6 \pm 0.8$	...	$13.5 \pm 1.6$
HHH86-C38=R123	$14.2 \pm 1.1$	...	...
HGHH92-C41	$11.5 \pm 1.3$	...	$9.6 \pm 2.0$
HGHH92-C44	$13.1 \pm 1.0$	...	$9.1 \pm 2.0$
HCH99-2	$14.1 \pm 0.5$	...	...
HCH99-15	$21.3 \pm 1.7$	...	...
HCH99-16	$9.5 \pm 1.4$	...	...
HCH99-18	$21.2 \pm 1.1$	...	...
HCH99-21	$10.6 \pm 2.3$	...	...
R122	$4.9 \pm 1.1$ :	...	...
R223	$14.4 \pm 1.5$	...	...
R261	$14.6 \pm 0.7$	...	...

has been derived for cluster HGHH92-C37 (R116) from our FORS1 data with respect to work of Harris et al. (2002). The difference in this particular case might be due to the location of the cluster close to the edge of FORS1 field, where image distortions could have affected the measurement. The very high ellipticity of R122 could be due to the fact that the image of this cluster is most probably blended with some foreground source (see also above). We have put ":" sign next to the ellipticity determinations from FORS1 data that are more uncertain.

## 5. Cluster masses and mass-to-light ratios

The masses and the mass-to-light ratios for all the clusters with the available (or new) structural parameter measurements are given in Table 6. The listed masses are virial masses calculated using the virial theorem in the form (Spitzer 1987):

$$M_{vir} \simeq 2.5 \frac{3\sigma^2 r_h}{G} \quad (4)$$

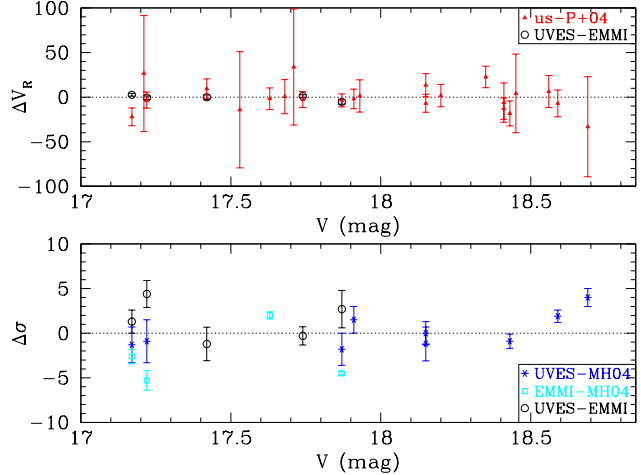


**Fig. 6.** Comparison of the measurements from the literature and our results, as well as comparison between UVES and EMMI measurements for the clusters in common. In the upper panel we plot the difference between radial velocity and in the lower panel velocity dispersion differences as a function of magnitude. In both panels the open circles are used to compare UVES and EMMI measurements. The filled triangles are comparing radial velocities with those of Peng et al. (2004a, P+04). In the lower panel our velocity dispersions are compared with those of Martini & Ho (2004, MH04) for clusters observed with UVES (asterisks) and EMMI (open squares) separately. (See the electronic edition of the journal for the colour version of this figure.)

where, assuming an isotropic velocity distribution,  $3\sigma^2$  is the mean square velocity of the stars and the cluster half-mass radius ( $r_h$ ) is related to the half-light (effective) radius ( $r_e$ ) through  $r_e \approx 3r_h/4$  (Spitzer 1987).

1" slit at the distance of 3.84 Mpc (Rejkuba 2004) corresponds to 18.62 pc. Seeing better than 0''.8 ensures that most of the light is in the slit. The central velocity dispersion  $\sigma_0$  has been estimated from the King profile fits convolved with the Gaussian of the width that reproduces the intensity profile with FWHM as measured along the spatial direction in the slit for each target (e.g. Djorgovski et al. 1997; Haşegan et al. 2005). The corrections from the observed to central  $\sigma$  range from 4–10%, with the average correction of  $\sim 6\%$  being valid for most of the clusters.

Core radii of Cen A clusters are typically smaller than the resolution element, even for space based imagers, and thus the quoted errors for  $r_c$  in Table 6 are probably underestimated. In addition, as stated before, the concentration parameter is also relatively uncertain, especially for the clusters that had structural parameters determined with ISHAPE. Therefore we prefer to use the virial mass estimator as described above, rather than deriving the masses using the King model approximation, which would imply using central velocity dispersion, core radius, and concentration parameter (Queloz et al. 1995). The uncertainty in structural parameters imply also that the corrections of the observed  $\sigma$  to the central value of velocity dispersion and to the infinite aperture  $\sigma$  are quite uncertain. In the

next section, when we plot  $\sigma_0$ , we apply a flat average correction of 6% for all the clusters.

In the calculation of the virial masses (Equ. 4)  $\sigma$  is the mean value of velocity dispersion averaged over the whole cluster. In all our targets 1" slit samples the light to at least  $3.5 r_c$ , and in most cases beyond  $6 r_c$ . Comparing with  $\omega$  Cen and 47 Tuc (Meylan et al. 1995; McLaughlin et al. 2006), the faint surface brightness and low velocity dispersion have negligible contribution beyond  $3-5 r_c$ , and consequently  $\sim 90-95\%$  of the light of the clusters is in the slit. The corrections from the observed  $\sigma$  to infinite apertures estimated using the seeing convolved King profiles, are of the order of few percent. We prefer not to apply these rather uncertain corrections, but rather use the observed  $\sigma$ , since the corrections are smaller than the uncertainty on our other parameters. The negative error-bars for mass and M/L ratios in Table 6 include the maximum estimated aperture correction.

As expected from the comparison of the velocity dispersion measurements, the derived masses for the clusters in common with the Martini & Ho (2004) sample are in good agreement with their virial masses for the targets in common. With more bright globular clusters our sample has a larger number of clusters with masses similar to, or larger than, the most massive Milky Way cluster  $\omega$  Cen ( $M_{virial} = 3 \times 10^6 M_\odot$  Meylan et al. 1995) and G1 in M31 ( $M_{virial} = 7.3 \times 10^6 M_\odot$  Meylan et al. 2001).

The mass-to-light ratios ( $M/L_V$ ) are computed by dividing the derived masses with the  $V$ -band luminosities ( $L_V$ ) which are calculated assuming the absolute  $V$  magnitude of the Sun to be  $M_{V,\odot} = +4.83$  mag:

$$L_V = 10^{[-0.4*(V-(m-M)_V-A_V-M_{V,\odot})]} \quad (5)$$

The derived  $M/L_V$  ratios for our sample of globular clusters range from 0.1 to 5.9. However, we note that the cluster with the lowest  $M/L_V$ , R01-122, is the one that displays contribution from (perhaps) stellar contaminants in its high resolution spectra (Fig. 5). Thus its luminosity is expected to be overestimated, which would then underestimate the  $M/L_V$  ratio. Excluding this cluster, the smallest  $M/L_V$  is 1.1 and the average is  $< M/L_V > = 2.9 \pm 1.4$ , like also observed by Martini & Ho (2004). These authors note that this value is larger than the average  $M/L_V$  of globular clusters in the Local Group galaxies and they explore the possible explanations for this, concluding that the difference is most probably real. Our analysis confirms their results. We discuss this further in Sect. 7.

The errors of in the mass and  $M/L_V$  determinations reported in Table 6 include the errors from the velocity dispersion measurements and half-mass radii, and the errors due to aperture corrections, but do not include any systematic errors due to modeling or assumptions on reddening and distance. We note that, assuming a smaller distance modulus to NGC 5128 as determined by Ferrarese et al. (2006), the  $M/L_V$  ratios would actually increase by 12% and increase the difference with respect to Local Group globular clusters.

The presence of a significant internal reddening in NGC 5128 would have the opposite effect. However, from the measurements of the equivalent widths of the interstellar NaD doublet we estimate that the extinction is con-

sistent with very little or no internal reddening within the galaxy except for HGHH93-C23 whose spectra display multiple and stronger NaD absorption lines (at different velocities). Furthermore for the inner clusters, which are expected to suffer the most dust reddening, the internal reddening values derived by Holland et al. (1999), are in all cases smaller than  $E(B-V) = 0.14$  mag, and mostly below 0.1 mag. Unfortunately the uncertainty of the relation between NaD and equivalent widths and  $E(B-V)$  coupled with our noisy spectra, which yield high uncertainty in the NaD line equivalent width measurements, does not allow us to determine accurate reddening directly from the spectra. For the inner clusters we adopt the de-reddened magnitudes from Holland et al. (1999) for the computation of the  $M/L_V$  ratios (Table 6). For HGHH93-C23 we assume an additional  $E(B-V) = 0.2$  mag due to dust internal to NGC 5128, while for all the other clusters only the foreground Milky Way extinction of  $A_V = 0.34$  mag is assumed (Schlegel et al. 1998).

## 6. Special clusters

### 6.1. Clusters with X-ray sources

Kraft et al. (2001), Minniti et al. (2004b), Peng et al. (2004a), and Voss & Gilfanov (2006) have studied the Chandra X-ray point sources matching NGC5128 globular clusters. Minniti et al. (2004b) concluded that X-ray sources tend to be located in redder clusters (more metal-rich) and also preferentially reside in more luminous (massive) globular clusters. Three of the clusters in the present sample have been flagged as X-ray point sources based on the Chandra observations. These are C23 with luminosity  $L_X = 1.10 \times 10^{38}$ , C21 with  $L_X = 1.79 \times 10^{37}$ , and C7 with  $L_X = 1.89 \times 10^{37}$ . Clusters C7 and C23 are the second and the third most massive, and C21 is sixth most massive cluster in our sample. According to the data of Peng et al. (2004a), these three clusters are red, with  $V-I = 1.1-1.3$ , and luminous, with  $V = 17.9$  to  $17.2$  (or  $M_V = -10.3$  to  $-11$ ). The X-ray luminosities of C21 and C7 are expected from typical low-mass X-ray binaries (LMXBs). The C23 luminosity puts this cluster on the bright tail of the distribution of X-ray point sources in NGC 5128 globular clusters shown in Figure 5 of Minniti et al. (2004b). This can be due to the presence of a couple of LMXBs in this massive cluster, or to a single ultra-compact binary (Bildsten & Deloye 2004). The alternative explanation of a more massive accreting BH cannot be excluded, but it is really not demanded by the available data. In this respect, C23 appears to be similar to the globular cluster Bo375 of M31, which contains the brightest X-ray point source in a spectroscopically confirmed globular cluster, with  $L_X = 2-6 \times 10^{38}$  (Di Stefano et al. 2002).

### 6.2. The most massive cluster

The brightest cluster of our sample is HCH99-18, with  $V = 17.07$ . This is also the most massive cluster, with  $M_{vir} = 1.4 \times 10^7 M_\odot$ , and the largest cluster in size (Table 6). It is apparently a metal-rich cluster, which has normal infrared colours (Minniti et al. 1996). It is located in the inner parts

**Table 7.** Properties of HCH99-18,  $\omega$  Cen and G1. The data for the last two clusters are from Meylan et al. (1995, 2001) and Harris (1996). The two ( $V - I$ ) colours of HCH99-18 are from HST photometry of Holland et al. (1999), and in parenthesis the measurement from Peng et al. (2004b) catalogue. The reddening towards this cluster is separated into foreground Galactic reddening (Schlegel et al. 1998), and internal reddening within NGC 5128 along the line of sight (Holland et al. 1999).

	HCH99-18	$\omega$ Cen	G1
$M_V$ (mag)	-11.38	-10.29	-10.94
$(B - V)$ (mag)	1.06	0.78	0.84
$(V - I)$ (mag)	0.99 (1.50)	1.05	
$E(B - V)$ (mag)	0.11 + 0.06	0.12	0.06
$\sigma_p(0)$ (km/s)	21.2	22	27.8
$r_c$ (pc)	1.2	4.6	0.52
$r_h$ (pc)	18.3	13	14
$c = \log r_h/r_c$	1.5	1.23	2.5
$\epsilon$	0.030	0.121	0.2
$M_{virial}$ ( $M_\odot$ )	$1.4 \times 10^7$	$3.0 \times 10^6$	$7.3 \times 10^6$
$M/L_V$	4.7	2.4	3.6
$R_{gc}$ (kpc)	1.5	6.4	40.1
[Fe/H]		-1.62	-0.95

of NGC 5128, only 1.5 kpc away from the galactic nucleus, where reddening might be a problem. The internal reddening due to dust in NGC 5128 in the line of sight to this cluster is  $E(V - I) = 0.1$  (i.e.  $E(B - V) = 0.06$ ) mag (Holland et al. 1999). This relatively low internal reddening is confirmed by the low total equivalent width of interstellar NaD lines. Its  $M/L_V$  ratio is 4.7, higher than those of  $\omega$  Cen ( $M/L_V = 2.4$ ) and G1 ( $M/L_V = 3.6$ ) globular clusters where the masses and  $M/L$  were always taken from the same method, virial theorem (Meylan et al. 2001). The ( $V - I$ ) colour of HCH99-18 taken from the original discovery work of Holland et al. (1999) is 0.99, significantly bluer than the ( $V - I$ ) = 1.50 in Peng et al. (2004b) catalogue.

For a straight forward comparison of this most massive cluster (so far) in NGC 5128, with the  $\omega$  Cen and G1 we summarize their main properties in Table 7. Data for  $\omega$  Cen and G1 are from Meylan et al. (1995, 2001) and Harris (1996). There is no available literature value for the spectroscopy of HCH99-18, but its redder colours indicate slightly higher metallicity if the same old age is assumed as for the other two clusters. This could explain the higher  $M/L_V$  value of this cluster. Its mass is factor of 2 larger than that of G1, the more massive of the two Local Group clusters.

As already mentioned in the introduction, one of the favoured formation scenarios for  $\omega$  Cen and G1 is being remnant nucleus of stripped dwarf galaxy. This scenario has been invoked to explain peculiar properties of these massive clusters, such as the presence of chemical inhomogeneities, the high flattening, and the high central velocity dispersion, among others (Zinnecker et al. 1988; Hughes & Wallerstein 2000; Hilker & Richtler 2000; Bekki & Freeman 2003; Bekki & Chiba 2004). While it is not possible to measure the presence or the absence of metallicity

dispersion in HCH99-18, the three clusters share similar properties, with the exception of low ellipticity. The ellipticity of HCH99-18 is actually similar to that of M 54 ( $\epsilon = 0.06$ ), another Galactic globular cluster which is also considered to be a former nucleus of a dwarf galaxy. Thus it is possible that HCH99-18 also formed in a similar way. The alternative formation scenario to that of a stripped dwarf galaxy nucleus, could be through a merger of two or more young clusters (Minniti et al. 2004a; Fellhauer & Kroupa 2002).

This object has the mass comparable to some of the most massive *young* massive clusters in galactic merger remnants, e.g. W3 and W30 in NGC 7252 and G114 in NGC 1613 (Maraston et al. 2004; Bastian et al. 2006). To the best of our knowledge it is the brightest and most massive *old* globular cluster known to date within the distance of Cen A, and has similar properties to compact massive objects like DGTOs/UCDs observed in the Virgo and Fornax clusters, and therefore it definitely warrants further study.

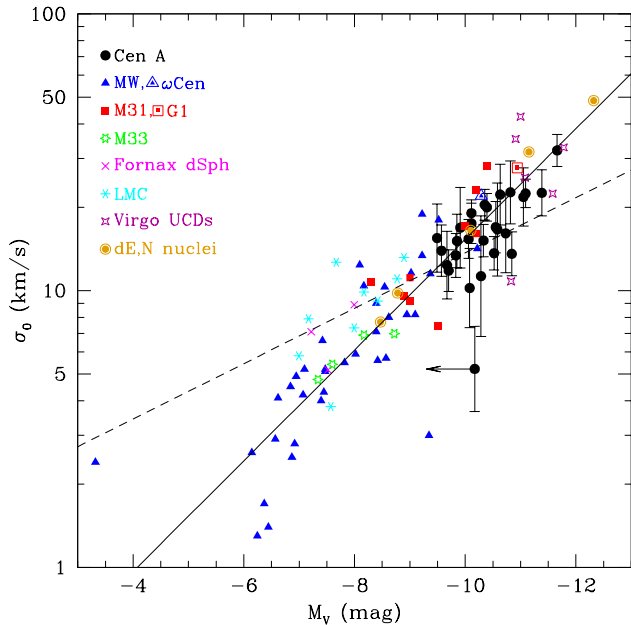
## 7. Discussion

Figure 7 shows the relation between the absolute  $V$  magnitude and velocity dispersion. The sources of the data compiled from the literature and shown together with our Cen A clusters for comparison are given in the caption of the figure. The dashed line is the Faber-Jackson relation (Faber & Jackson 1976) for bright ellipticals, while the solid line shows the best fit relation for Galactic globular clusters from McLaughlin & van der Marel (2005).

The bright globular clusters in NGC 5128 extend the globular cluster luminosity-velocity dispersion relation towards brighter objects like DGTOs and nucleated dwarf elliptical (dE,N) galaxy nuclei.

Figures 8, 9 and 10 display the relations between mass and velocity dispersion, mass-to-luminosity and effective (half-light) radius, respectively. Our bright clusters in NGC 5128 (Cen A) are plotted together with typical old ( $age > 10$  Gyr) globular clusters from Local Group galaxies: Milky Way, LMC, Fornax dSph, M31 and M33. For comparison we also plot the transition objects between the globular clusters and dwarf galaxies: DGTOs (Haşegan et al. 2005) and nuclei of dE,N (Geha et al. 2002). The solid lines are the best fit mass-sigma relation for globular clusters, the average dynamically determined  $M/L = 1.45$  (McLaughlin 2000), and median  $r_e = 3.2$  pc, which are for Galactic globular clusters independent of mass (McLaughlin & van der Marel 2005). The dashed lines are the best fit relations for bright elliptical galaxies as discussed by Haşegan et al. (2005).

In all the above figures (7–10) for comparison we also show the locations of the brightest Milky Way cluster  $\omega$  Cen and M31 cluster G1. Since the masses of our clusters were obtained using the virial theorem, we plot virial masses where available: for  $\omega$  Cen, G1, and M33 clusters. However, the literature source for the other Milky Way clusters, as well as clusters in the LMC, SMC and Fornax (McLaughlin & van der Marel 2005), presents only masses derived from King model fits, and the same is true for the masses of Virgo cluster DGTOs (Haşegan et al. 2005). The masses of dE,N galaxy nuclei result



**Fig. 7.** Central velocity dispersion versus absolute  $V$  band magnitude relation for globular clusters in NGC 5128 (Cen A; black filled circles, this work) is compared with old ( $age > 10$  Gyr) clusters in Local Group galaxies as well as with transition objects between globular clusters and dwarf galaxies, UCDs/DGTOs from the work of Haşegan et al. (2005) and nuclei of dwarf ellipticals in Virgo (Geha et al. 2002). The sources of data for the Local Group clusters are as follows: the Milky Way, Fornax dSph and LMC clusters are from McLaughlin & van der Marel (2005), M31 from Dubath & Grillmair (1997), M33 from Larsen et al. (2002), G1 cluster data are from Meylan et al. (2001) and  $\omega$  Cen from Meylan et al. (1995). For clarity error-bars are omitted for all but our data. They include the uncertainties in the correction from observed to central  $\sigma$ . The outlying cluster from our sample, R01-122 has its luminosity overestimated due to probable blend with foreground stars, as indicated by the arrow. The dashed line is the Faber-Jackson relation (Faber & Jackson 1976) for bright ellipticals, while the solid line shows the best fit relation for Galactic globular clusters from McLaughlin & van der Marel (2005). (See the electronic edition of the journal for the colour version of this figure.)

from dynamical modeling (Geha et al. 2002). When comparing these different systems we caution that Meylan et al. (2001) pointed out that the masses from King model fits are twice as large (however for counter example see Larsen et al. 2002).

In Fig. 8 the departure from the scaling relation for globular clusters becomes evident. The brightest clusters in NGC 5128 and dE,N nuclei occupy the same part of the diagram, which is shared also by some, but not all UCDs/DGTOs. However, as discussed by Haşegan et al. (2005) DGTOs from their sample have probably different formation mechanisms and thus different properties, with some being more similar to typical globular clusters and others either stripped galactic nuclei or merged complexes of star clusters.

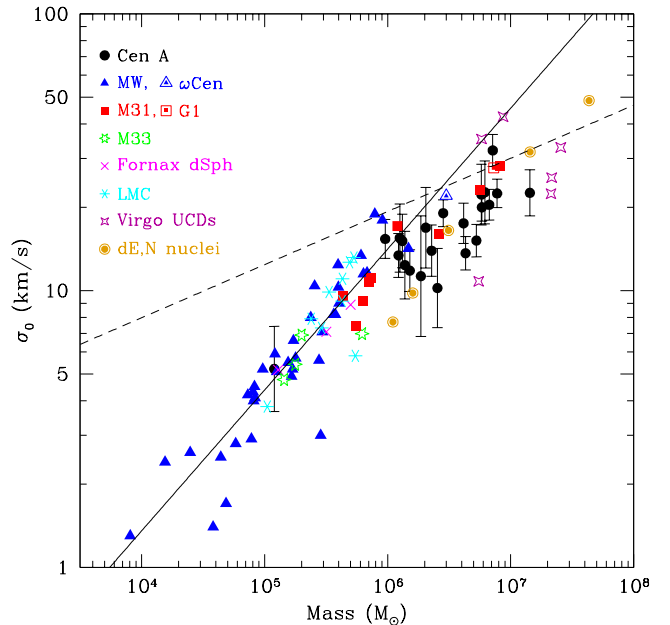


**Fig. 8.** Central velocity dispersion is plotted as a function of mass. For the literature sources for the clusters from the Local Group galaxies and UCDs/DGTOs and dE,N nuclei from Virgo clusters (see caption of Fig. 7). Solid line shows the virial theorem for globular clusters and the dashed line is a dependence between mass and  $\sigma$  for bright elliptical galaxies (Equ. 13 and 12 from Haşegan et al. 2005). (See the electronic edition of the journal for the colour version of this figure.)

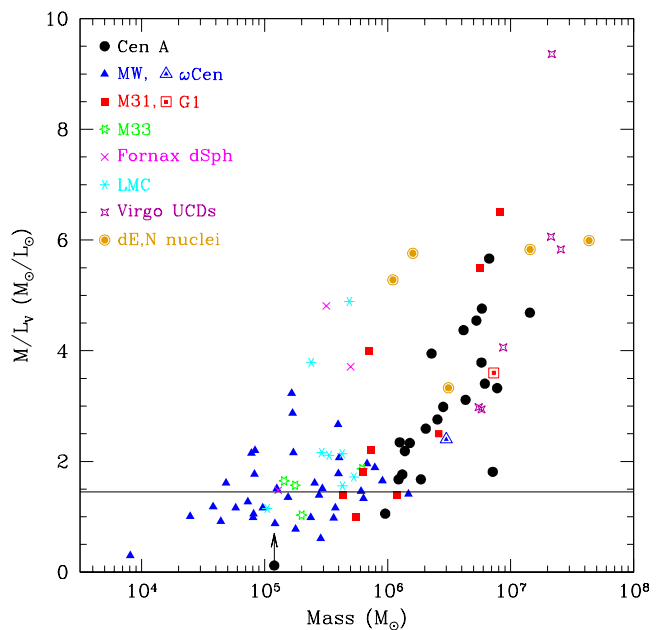


**Fig. 9.** Same as Fig. 8, but for mass-to-luminosity as a function of mass. Solid line shows the average dynamically determined  $M/L = 1.45$  for a sample of Galactic globular clusters (McLaughlin 2000). (See the electronic edition of the journal for the colour version of this figure.)

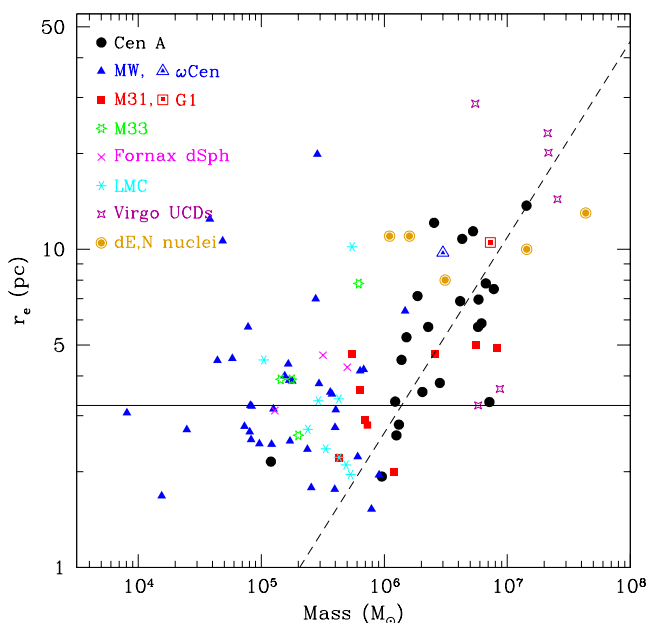


**Fig. 10.** Same as Fig. 8, but for effective (half-light) radius as a function of mass. Solid line shows the median  $r_e = 3.2$  pc for Galactic globular clusters, while the dashed line shows the dependence between mass and effective (half-light) radius for bright elliptical galaxies (Equ. 12 from Haşegan et al. 2005). (See the electronic edition of the journal for the colour version of this figure.)

While the lower mass clusters do not show dependence of the M/L on the mass, a quite clear relation emerges for the clusters with masses larger than  $\sim 2 \times 10^6 M_\odot$  (Fig. 9). This is similar to the nuclei of dwarf galaxies, and UCDs/DGTOs (Geha et al. 2002; Haşegan et al. 2005) and is also obeyed by the most massive clusters in the Milky Way (e.g.  $\omega$  Cen; framed blue triangle) and in M31 (e.g. G1; red framed square).

All Local Group globular clusters plotted in these scaling relation diagrams have ages in excess of 10 Gyr. The ages of Cen A clusters are not well known. Peng et al. (2004b) found that the metal-poor bright Cen A clusters have ages similar to those of Milky Way clusters, while the metal-rich appear younger with ages up to 5 Gyr. Since the  $M/L_V$  of a population of a given age increases with metallicity, it is in principle possible to construct a sample where the more massive globular clusters would be more metal-rich, thus having also higher  $M/L$  ratios. However we note that no relation between the  $(V - I)_0$ , nor  $(B - V)_0$  colour and  $M/L$  is present neither in our data (Figure 11) nor was noted by Martini & Ho (2004).

Individual spectroscopic metallicities are not available for Cen A clusters in the literature. Therefore to explore the age-metallicity dependence on M/L ratio we use  $(B - V)_0$  and  $(V - I)_0$  colours and compare them to Maraston (2005) models in Figure 11. In the upper panels we plot the models for Kroupa (2001) initial mass function (IMF), while the bottom panels have models calculated with Salpeter (1955) IMF. Looking only at the Cen A clusters (filled dots with error-bars), the models with Salpeter IMF reproduce the range of M/L ratios indi-

cating that the clusters with high M/L ratios are old and metal-rich. This result is very similar to that found for Fornax cluster UCDs by Hilker et al. (2007). However, we point out that these models predict too high M/L ratios with respect to the MW *old* globular cluster M/Ls. Models with Kroupa IMF pass through the region occupied by MW globulars, but they still imply too young ages for most of them. Bruzual & Charlot (2003) models with Chabrier (2003) IMF have lower M/L ratios and thus fit better the range of M/L values of MW globular clusters (e.g. see Fig. 11 of Haşegan et al. (2005) and Fig. 11 of Hilker et al. (2007)). However, these models do not cover the part of the plane where Cen A clusters lie. In principle, it is therefore possible by choosing the IMF and different simple stellar population models to find a good solution for either Cen A clusters or MW clusters, but not both.

The average colours of our sample of clusters in NGC 5128 are  $< (B - V)_0 > = 0.81 \pm 0.07$  mag and  $< (V - I)_0 > = 0.94 \pm 0.10$  mag. This is respectively 0.14 and 0.07 mag redder than the average colours of the MW globulars that we use for comparison in Figure 11. Assuming that all the clusters have the same old age, the higher average  $M/L_V$  ratio for the clusters in Cen A with respect to those in MW can be explained in part with their higher metallicity. However, even excluding the reddest clusters from our sample, the average  $M/L_V$  ratio of the bright clusters in Cen A is still on average higher than that of "normal" globular clusters. As can be seen from Figure 9 their M/L ratios cover a range between those of "normal" globular clusters and those of UCDs and dE,N nuclei.

We note also that the half-light radius is independent of the mass for the low mass clusters, while it increases with the mass for clusters more massive than  $\sim 2 \times 10^6 M_\odot$ . This shows that, bright, massive clusters present a transition type of objects between typical globular clusters and more massive DGTOs and dE,N nuclei. The implications of this finding for the *young* massive clusters has been discussed in detail by Kissler-Patig et al. (2006). They have argued for the possibility of formation of such massive objects through early mergers of low mass stellar clusters, which might explain the emergence of mass-radius relation (for more details see Kissler-Patig et al. (2006) and references therein). As an alternative speculation Kissler-Patig and collaborators suggest a possibility that "all star clusters form with a primordial mass-radius relation, but only the most massive clusters are able to retain it against the processes that would erase it". The result presented in Figure 10 is consistent with the latter scenario, which should be further explored theoretically.

Another parameter that might be linked to the formation scenario is ellipticity. The high ellipticity of  $\omega$  Cen in our Galaxy and G1 in M31 have been frequently mentioned together with other peculiarities shared by these two clusters, in the context of the stripped galaxy nucleus formation mechanism (e.g. Bekki & Freeman 2003; Bekki & Chiba 2004). Large fraction of the massive clusters in M31, LMC, and some in the MW show significant ellipticities (Geisler & Hodge 1980; Harris 1996; Barmby et al. 2000). Ellipticities of Cen A clusters have been compared to those of MW globular clusters and discussed by Holland et al. (1999), Harris et al. (2002), and Gómez et al. (2006). They found a strikingly high fraction of

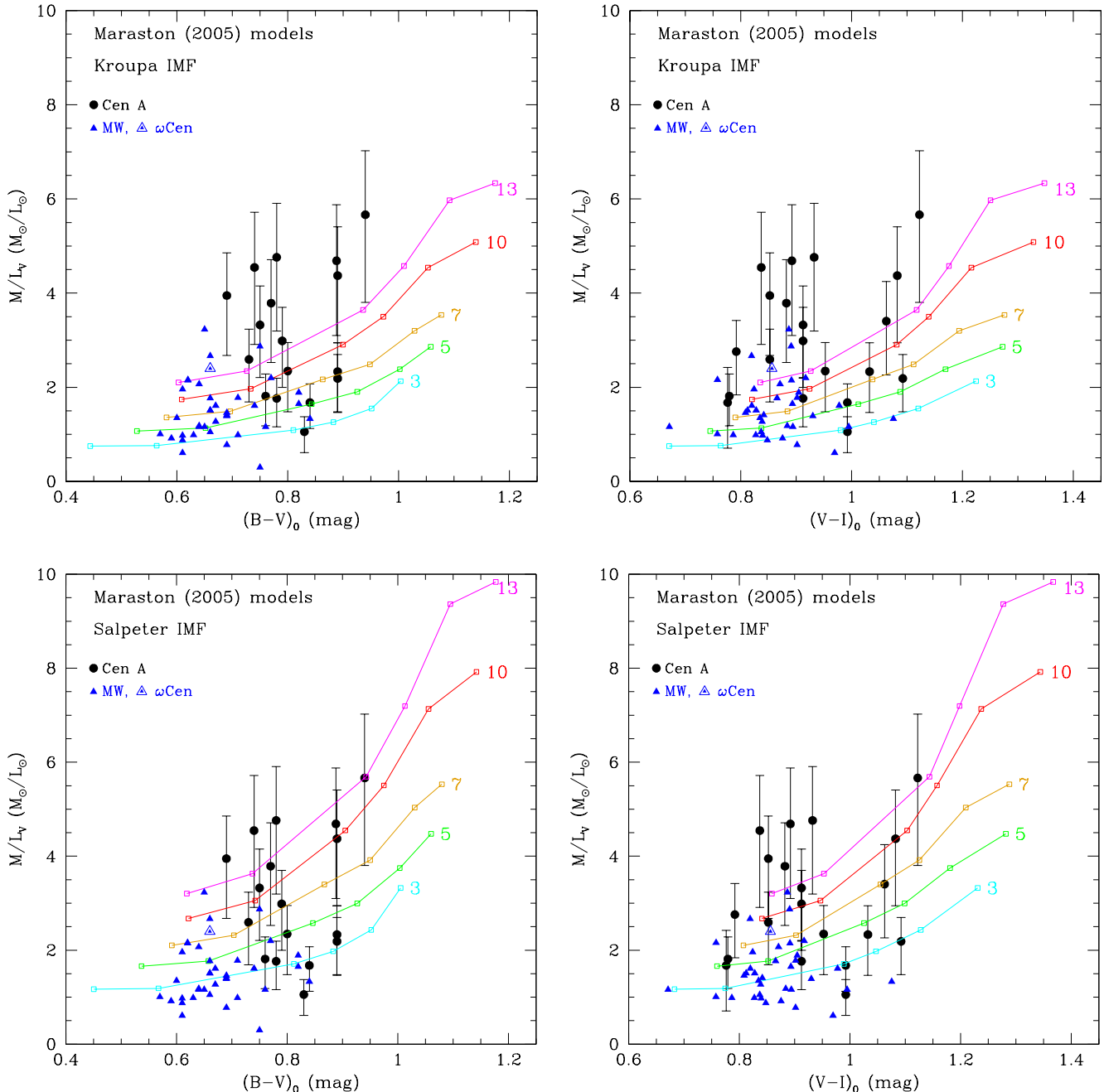


**Fig. 11.** The measured M/L ratios as a function of de-reddened  $(B - V)$  (left) and  $(V - I)$  (right) colours for our sample of clusters in Cen A, and old globular clusters in the MW, are compared to expected values from SSP models of Maraston (2005) computed for two different IMFs, as shown in each panel. The ages of the theoretical predictions are shown on to the right of the curves. The model colours (open squares) from blue to red are for the following metallicities:  $[Z/H] = -2.25, -1.35, -0.33, 0.0, +0.35$  and  $0.67$  dex. The colours of MW clusters are taken from Harris (1996) web<sup>2</sup> catalogue. (See the electronic edition of the journal for the colour version of this figure.)

very elongated clusters among the luminous clusters in Cen A. Since our sample contains most of the clusters already examined by these authors, it is not surprising to reach similar conclusions. In addition to comparing the ellipticities of clusters as a function of luminosity we can test whether there is any dependence of ellipticity on the mass of the cluster - in our sample we find none.

In a recent paper Fellhauer & Kroupa (2006) argue that the tidal heating during a close passage to the galactic center of a UCD may squeeze the velocity distribution of its stars and therefore lead to an overestimation of virial mass and M/L ratio. In these simulations the more compact and the more massive the object, the smaller is the effect on the measured velocity dispersion. For the models similar to the UCDs in Virgo and Fornax

clusters, with core radii of the order of 25 pc and masses of  $10^7 M_{\odot}$ , only those that pass within 100–1000 pc from the center of galaxy can be significantly affected by tidal heating.

In Table 6 we list in column 7 the projected galactocentric distance for the clusters in our sample. No correlation between the mass or M/L ratio and the galactocentric distance is observed. While without additional simulations it is not clear if and by how much tidal heating could be affecting the velocity dispersion measurements and thus mass determinations in the relatively (with respect to UCDs) compact globular clusters, we cannot exclude a possibility that some of the clusters have their masses overestimated due to inadequate assumption of virial equilibrium. However, given the range of masses, galactocentric distances and the relatively compact clusters, the explanation of the mass– $M/L_V$  relation (Fig. 9) is unlikely to be due to systematic overestimation of mass and  $M/L_V$  due to the tidal heating of the clusters. This relation might instead be connected to the formation mechanism.

## 8. Conclusions

We have presented an analysis of the radial velocities and velocity dispersions for 27 bright globular clusters in the nearby elliptical galaxy NGC 5128. For two targets we have confirmed here for the first time their membership in NGC 5128 through radial velocity measurements. Also, for 7 clusters we present the first measurements of their structural parameters from the King profile fitting to the high resolution ground based images.

For 22 clusters we combine our new velocity dispersion measurements with the information on the structural parameters, either from the literature when available or from our own data, and use the virial theorem to derive the cluster masses. The masses range from  $1.2 \times 10^5 M_{\odot}$ , typical of Galactic globular clusters, to  $1.4 \times 10^7 M_{\odot}$ , similar to more massive DGTOs and nuclei of dE,N galaxies.

HCH99-18 is the brightest and the most massive cluster in our sample with  $M_{vir} = 1.4 \times 10^7 M_{\odot}$ . With such a high mass and the  $M/L_V$  ratio of 4.7 it is a candidate for being the remnant nucleus of a stripped dwarf galaxy. The alternative explanation could be the merger of two or more young clusters (Minniti et al. 2004a). To the best of our knowledge it is the brightest and most massive *old* globular cluster known to date within the distance of Cen A, and it shares similar properties with compact massive objects like DGTOs/UCDs observed in the Virgo and Fornax clusters. Therefore it definitely warrants further study.

The most striking finding of our study is the emergence of the mass–radius and the mass– $M/L_V$  relations for the bright clusters with masses larger than  $\sim 2 \times 10^6 M_{\odot}$ . Figure 9 hints to the possible existence of two “populations” of globular clusters: (1) less massive (“normal”) globular clusters, like the ones found typically in the Milky Way and M33, with  $M/L_V$  roughly independent of the mass, and (2) brighter more massive clusters, including our targets from Cen A as well as  $\omega$  Cen and G1, with  $M/L_V$  ratios that seem to increase with increasing mass. Moreover, population 2 seems to link population 1 with more massive objects such as UCDs and dE,N nuclei. Figure 10, although less clearly, suggests another difference between

the population 1 with effective radius independent of mass, and population 2 with radius increasing with mass.

This has been previously discussed for the *young* massive clusters (Kissler-Patig et al. 2006) in galactic mergers and for DGTOs in the Virgo cluster (Haşegan et al. 2005). Our results indicate that the bright, massive, globular clusters associated with elliptical galaxies might present the missing link between “normal” old globular clusters associated with galaxies, *young* massive clusters formed in mergers and evolved massive objects like UCDs (or DGTOs) associated with galaxy clusters.

**Acknowledgements.** MR is grateful to Soeren Larsen for helpful hints and discussions and acknowledge discussions with the cross-correlation gurus of the Geneva Observatory, in particular Stephane Udry and Didier Queloz. Many thanks to Andres Jordán for interesting discussions and help with estimating aperture corrections. MR is also grateful for a stay at the Observatoire de Sauverny supported by EPFL. DM is supported by FONDAP Center for Astrophysics 15010003 and by a Fellowship from the John Simon Guggenheim Foundation. We thank an anonymous referee for the careful reading of the manuscript and suggestions for improvement.

## References

- Ballester, P., Boitquin, O., Modigliani, A., & Wolf, S. 2000, UVES Pipeline User’s Manual, vlt-man-eso-19500-2964 edn.
- Barmby, P., Huchra, J. P., Brodie, J. P., et al. 2000, AJ, 119, 727
- Bassino, L. P. & Muzzio, J. C. 1995, The Observatory, 115, 256
- Bastian, N., Saglia, R. P., Goudfrooij, P., et al. 2006, A&A, 448, 881
- Bekki, K. & Chiba, M. 2004, A&A, 417, 437
- Bekki, K. & Freeman, K. C. 2003, MNRAS, 346, L11
- Bevington, P. R. 1969, Data Reduction and error analysis for the physical sciences (New York: McGraw-Hill)
- Bildsten, L. & Deloye, C. J. 2004, ApJ, 607, L119
- Bruzual, G. & Charlot, S. 2003, MNRAS, 344, 1000
- Chabrier, G. 2003, PASP, 115, 763
- Cohen, J. G. 2006, ApJ, 653, L21
- de Medeiros, J. R. & Mayor, M. 1999, A&AS, 139, 433
- Dekker, H., Delabre, B., & Dodorico, S. 1986, in Instrumentation in astronomy VI; Proceedings of the Meeting, Tucson, AZ, Mar. 4-8, 1986. Part 1 (A87-36376 15-35). Bellingham, WA, Society of Photo-Optical Instrumentation Engineers, 1986, p. 339-348., ed. D. L. Crawford, 339–348
- Dekker, H., D’Odorico, S., Kaufer, A., Delabre, B., & Kotzlowski, H. 2000, in Proc. SPIE Vol. 4008, p. 534-545, Optical and IR Telescope Instrumentation and Detectors, Masanori Iye; Alan F. Moorwood; Eds., ed. M. Iye & A. F. Moorwood, 534–545
- Di Stefano, R., Kong, A. K. H., Garcia, M. R., et al. 2002, ApJ, 570, 618
- Djorgovski, S. & Meylan, G. 1994, AJ, 108, 1292
- Djorgovski, S. G., Gal, R. R., McCarthy, J. K., et al. 1997, ApJ, 474, L19+
- Drinkwater, M. J., Jones, J. B., Gregg, M. D., & Phillipps, S. 2000, Publications of the Astronomical Society of Australia, 17, 227

Dubath, P. 1994, Bulletin of the American Astronomical Society, 26, 1398

Dubath, P. & Grillmair, C. J. 1997, A&A, 321, 379

Dubath, P., Meylan, G., & Mayor, M. 1992, ApJ, 400, 510

Dubath, P., Meylan, G., & Mayor, M. 1997, A&A, 324, 505

Dubath, P., Meylan, G., Mayor, M., & Magain, P. 1990, A&A, 239, 142

Faber, S. M. & Jackson, R. E. 1976, ApJ, 204, 668

Famaey, B., Jorissen, A., Luri, X., et al. 2005, A&A, 430, 165

Fellhauer, M. & Kroupa, P. 2002, MNRAS, 330, 642

Fellhauer, M. & Kroupa, P. 2006, MNRAS, 367, 1577

Ferrarese, L., Mould, J. R., Stetson, P. B., et al. 2006, ArXiv Astrophysics e-prints

Geha, M., Guhathakurta, P., & van der Marel, R. P. 2002, AJ, 124, 3073

Geisler, D. & Hodge, P. 1980, ApJ, 242, 66

Gómez, M., Geisler, D., Harris, W. E., et al. 2006, A&A, 447, 877

Haşegan, M., Jordán, A., Côté, P., et al. 2005, ApJ, 627, 203

Harris, G. L. H., Geisler, D., Harris, H. C., & Hesser, J. E. 1992, AJ, 104, 613

Harris, W. E. 1996, AJ, 112, 1487

Harris, W. E., Harris, G. L. H., Holland, S. T., & McLaughlin, D. E. 2002, AJ, 124, 1435

Hesser, J. E., Harris, H. C., & Harris, G. L. H. 1986, ApJ, 303, L51

Hesser, J. E., Harris, H. C., van den Bergh, S., & Harris, G. L. H. 1984, ApJ, 276, 491

Hilker, M., Baumgardt, H., Infante, L., et al. 2007, A&A, 463, 119

Hilker, M., Infante, L., Vieira, G., Kissler-Patig, M., & Richtler, T. 1999, A&AS, 134, 75

Hilker, M. & Richtler, T. 2000, A&A, 362, 895

Holland, S., Côté, P., & Hesser, J. E. 1999, A&A, 348, 418

Hughes, J. & Wallerstein, G. 2000, AJ, 119, 1225

King, I. R. 1962, AJ, 67, 471

King, I. R. 1966, AJ, 71, 64

Kissler-Patig, M., Jordán, A., & Bastian, N. 2006, A&A, 448, 1031

Kraft, R. P., Kregenow, J. M., Forman, W. R., Jones, C., & Murray, S. S. 2001, ApJ, 560, 675

Kroupa, P. 2001, MNRAS, 322, 231

Larsen, S. S. 1999, A&AS, 139, 393

Larsen, S. S. 2001, AJ, 122, 1782

Larsen, S. S., Brodie, J. P., Sarajedini, A., & Huchra, J. P. 2002, AJ, 124, 2615

Layden, A. C. & Sarajedini, A. 2000, AJ, 119, 1760

Ma, J., de Grijs, R., Yang, Y., et al. 2006, MNRAS, 368, 1443

Maraston, C. 2005, MNRAS, 362, 799

Maraston, C., Bastian, N., Saglia, R. P., et al. 2004, A&A, 416, 467

Martini, P. & Ho, L. C. 2004, ApJ, 610, 233

McLaughlin, D. E. 2000, ApJ, 539, 618

McLaughlin, D. E., Anderson, J., Meylan, G., et al. 2006, ApJS, 166, 249

McLaughlin, D. E. & van der Marel, R. P. 2005, ApJS, 161, 304

Meylan, G., Mayor, M., Duquennoy, A., & Dubath, P. 1995, A&A, 303, 761

Meylan, G., Sarajedini, A., Jablonka, P., et al. 2001, AJ, 122, 830

Minniti, D., Alonso, M. V., Goudfrooij, P., Jablonka, P., & Meylan, G. 1996, ApJ, 467, 221

Minniti, D., Rejkuba, M., Funes, J. G., & Kennicutt, Jr., R. C. 2004a, ApJ, 612, 215

Minniti, D., Rejkuba, M., Funes, S. J., & Akiyama, S. 2004b, ApJ, 600, 716

Munari, U. & Zwitter, T. 1997, A&A, 318, 269

Nordström, B., Mayor, M., Andersen, J., et al. 2004, A&A, 418, 989

Norris, J. E. & Da Costa, G. S. 1995, ApJ, 447, 680

Olszewski, E. W., Pryor, C., & Armandroff, T. E. 1996, AJ, 111, 750

Pancino, E., Pasquini, L., Hill, V., Ferraro, F. R., & Bellazzini, M. 2002, ApJ, 568, L101

Peng, E. W., Ford, H. C., & Freeman, K. C. 2004a, ApJS, 150, 367

Peng, E. W., Ford, H. C., & Freeman, K. C. 2004b, ApJ, 602, 705

Queloz, D., Dubath, P., & Pasquini, L. 1995, A&A, 300, 31

Rejkuba, M. 2001, A&A, 369, 812

Rejkuba, M. 2004, A&A, 413, 903

Salpeter, E. E. 1955, ApJ, 121, 161

Schlegel, D. J., Finkbeiner, D. P., & Davis, M. 1998, ApJ, 500, 525

Spitzer, L. 1987, Dynamical evolution of globular clusters (Princeton, NJ, Princeton University Press, 1987, 191 p.)

Tonry, J. & Davis, M. 1979, AJ, 84, 1511

Udry, S., Mayor, M., & Queloz, D. 1999, in ASP Conf. Ser. 185: IAU Colloq. 170: Precise Stellar Radial Velocities, ed. J. B. Hearnshaw & C. D. Scarfe, 367-+

van den Bergh, S., Hesser, J. E., & Harris, G. L. H. 1981, AJ, 86, 24

Voss, R. & Gilfanov, M. 2006, A&A, 447, 71

White, R. E. & Shawl, S. J. 1987, ApJ, 317, 246

Willmarth, D. & Barnes, J. 1994, A User's Guide to Reducing Echelle Spectra With IRAF

Zinnecker, H., Keable, C. J., Dunlop, J. S., Cannon, R. D., & Griffiths, W. K. 1988, in IAU Symp. 126: The Harlow-Shapley Symposium on Globular Cluster Systems in Galaxies, ed. J. E. Grindlay & A. G. D. Philip, 603-+